DOI: https://doi.org/10.2138/am-2024-9435. http://www.minsocam.org/

Revision 1

# Rubinite, $Ca_3Ti^{3+}{}_2Si_3O_{12}$, a new mineral in CV3 carbonaceous chondrites and a refractory garnet from the solar nebula

Chi Ma[1,*], Takashi Yoshizaki[2], Alexander N. Krot[3], John R. Beckett[1], Tomoki Nakamura[2], Kazuhide Nagashima[3], Jun Muto[4], Marina A. Ivanova[5], Alexander A. Ulyanov[6]

[1]Division of Geological and Planetary Sciences, California Institute of Technology, Pasadena, CA 91125, USA
[2]Department of Earth Science, Graduate School of Science, Tohoku University, Aoba, Sendai, Miyagi 980-8578, Japan
[3]Hawai‘i Institute of Geophysics and Planetology, University of Hawai‘i at Mānoa, Honolulu, HI 96822, USA
[4]Division of Geoenvironmental Science, Graduate School of Science, Tohoku University, Aoba, Sendai, Miyagi 980-8578, Japan
[5]Vernadsky Institute, Kosygin St. 19, Moscow 119991, Russia
[6]Department of Geology, Moscow State University, Moscow 119992, Russia

## ABSTRACT

Rubinite (IMA 2016-110) is a recently discovered $Ti^{3+}$-dominant refractory mineral in the garnet group from the solar nebula. It has the $Ia\bar{3}d$ garnet-type structure with $a$ = 12.19(1) Å, and $Z$ = 8, and end-member formula of $Ca_3Ti^{3+}{}_2Si_3O_{12}$. Rubinite was identified as micrometer-sized crystals in five refractory Ca,Al-rich inclusions (CAIs) from the CV3 carbonaceous chondrites Allende, Efremovka, and Vigarano. In the Vigarano CAI *V3*, it occurs in the central portion of an ultrarefractory fragment with Zr,Y,Sc-oxide, spinel and davisite-diopside, all enclosed within an amoeboid olivine aggregate. In the Allende Compact Type A (CTA) CAI *AE01-01*, it occurs with gehlenitic melilite, perovskite, spinel, hibonite, davisite, grossmanite, and diopside. In Efremovka, rubinite occurs within gehlenitic melilite with perovskite, spinel, and grossmanite in three CTA CAIs *E101*, *E105*, and *40E-1* (in a compound CAI). Rubinite is present in spinel-poor regions in all four of the

Efremovka and Allende CAIs but it is in contact with spinel in the Vigarano inclusion.

The mean chemical composition of type rubinite in Allende is (in wt%) CaO 32.68, $Ti_2O_3$ 14.79, $TiO_2$ 13.06, $SiO_2$ 28.37 $Al_2O_3$ 3.82, $Sc_2O_3$ 1.80, $Na_2O$ 1.01, $ZrO_2$, 0.80, MgO 0.79, $V_2O_3$ 0.61, FeO 0.53, $Y_2O_3$ 0.07, $Cr_2O_3$ 0.05, total 98.38, giving rise to an empirical formula of $(Ca_{2.94}Na_{0.08})(Ti^{3+}_{1.04}Ti^{4+}_{0.59}Sc_{0.13}Mg_{0.10}V_{0.04}Fe_{0.04}Zr_{0.03})(Si_{2.38}Al_{0.38}Ti^{4+}_{0.24})O_{12}$, where $Ti^{3+}$ and $Ti^{4+}$ are partitioned based on stoichiometry. Efremovka rubinite has a similar composition with a mean empirical formula of $(Ca_{2.97}Na_{0.06})(Ti^{3+}_{1.05}Ti^{4+}_{0.66}Mg_{0.12}Sc_{0.09}Zr_{0.03}V_{0.03}Y_{0.01}Fe_{0.01})(Si_{2.36}Al_{0.48}Ti^{4+}_{0.16})O_{12}$. Vigarano rubinite is much more Y-, Sc-, and Zr-rich, having an empirical formula of $(Ca_{1.89}Y_{0.83}Mg_{0.28})(Ti^{3+}_{0.59}Sc_{0.50}Zr_{0.72}Mg_{0.2}V_{0.02}Cr_{0.01})(Si_{1.64}Al_{1.18}Ti^{4+}_{0.07}Fe_{0.06})O_{12}$. All rubinites are $Ti^{3+}$-rich but a significant amount (11–46%) of the Ti is $4^{+}$.

In the Efremovka CTAs, spinel is $^{16}O$-rich ($\Delta^{17}O$ ~ –24‰); rubinite and perovskite show limited ranges of $\Delta^{17}O$ (from –24 to –16‰; most analyses range from –24 to –20‰); melilite and grossmanite are the most $^{16}O$-depleted minerals ($\Delta^{17}O$ range from ~ –10 to –4‰ and from –8 to –5‰, respectively). In the Allende CTA *AE01-01*, spinel and hibonite are $^{16}O$-rich ($\Delta^{17}O$ ~ –24‰); melilite, rubinite and perovskite show large ranges in $\Delta^{17}O$ (from –23 to –3‰, from –21 to –6‰, and from –14 to –2‰, respectively); grossmanite is uniformly $^{16}O$-depleted ($\Delta^{17}O$ ~ –3‰).

Rubinite formed under highly reducing conditions in the solar nebula by gas-solid condensation and by crystallization from a Ca, Al, and Ti-rich melt. Subsequently, most rubinite grains in the Allende CAI and some in the Efremovka CAIs may have experienced O-isotope exchange to a various degree with an $^{16}O$-depleted ($\Delta^{17}O$ ~ –2‰) aqueous fluid on the CV chondrite parent asteroid. However, crystallization from a Ca,Al,Ti-rich melt that recorded O-isotope exchange: with nebular gas with variable $\Delta^{17}O$ or post-crystallization O-isotope with such gas cannot be excluded.

The mineral name is in honor of Alan E. Rubin (b. 1953), a cosmochemist at University of California, Los Angeles (UCLA), USA, for his many contributions to research in cosmochemistry and mineralogy of meteorites.

**Keywords**: Rubinite; $Ca_3Ti^{3+}{}_2Si_3O_{12}$; refractory mineral; Vigarano; Allende; Efremovka; CV carbonaceous chondrites; refractory inclusions; oxygen isotopes; eringaite; garnet.

*E-mail: chima@caltech.edu

## INTRODUCTION

Refractory minerals in Ca-, Al-rich inclusions (CAIs) and amoeboid olivine aggregates (AOAs) from carbonaceous chondrites are the first solids formed in the Solar System, providing evidence for the earliest high-temperature processes in the solar nebula. To date, more than 50 refractory and ultrarefractory minerals have been identified, marking the very beginning of solar mineral evolution (Rubin and Ma 2021). Twenty eight of them are Ti-rich refractory phases (Table 1), including 15 recently-discovered minerals from carbonaceous chondrites like grossmanite [$Ca(Ti^{3+},Sc,Al,Mg)AlSiO_6$] (Ma and Rossman 2009b), tistarite ($Ti_2O_3$) (Ma and Rossman 2009c), panguite [$(Ti^{4+},Al,Sc,Mg,Zr,Ca)_{1.8}O_3$] (Ma et al. 2012), machiite [$(Al,Sc)_2(Ti^{4+},Zr)_3O_9$] (Krot et al. 2020), kaitianite ($Ti^{3+}{}_2Ti^{4+}O_5$) (Ma and Beckett 2021), and paqueite [$Ca_3Ti^{4+}Si_2(Al,Ti^{4+},Si)_3O_{14}$] (Ma et al. 2022). Titanium as a structural essential element or substitute in refractory and ultrarefractory phases is an important indicator of environment and process at high temperatures in the early Solar System. In addition, secondary Ti-rich garnet, hutcheonite [$Ca_3Ti^{4+}{}_2(SiAl_2)O_{12}$], was described in a CAI from the CV3 carbonaceous chondrite Allende (Ma and Krot 2014). Each of these new minerals adds a piece to the puzzle of understanding nebular and asteroidal processes that affected CAIs.

In this work, we describe rubinite – a new titanium garnet mineral, $Ca_3Ti^{3+}{}_2Si_3O_{12}$, which has a garnet-type structure, in five refractory CAIs from three carbonaceous chondrites – Vigarano (CV3.1–3.4 breccia), Allende ($CV_{ox}$>3.6), and Efremovka ($CV_{red}$3.1–3.4) (Bonal et al. 2006). Electron probe microanalysis (EPMA), scanning electron microscopy (SEM), electron backscatter diffraction (EBSD), micro-Raman, and secondary ion mass spectrometry (SIMS) were used to characterize the chemical compositions, structures, and oxygen-isotope compositions of this mineral and coexisting phases. Preliminary results are given by Ma et al.

(2017c). Preliminary investigation of mineralogy and oxygen isotopic composition of minerals from UR CAI *40E-1* were reported by Ivanova et al. (2017).

## SAMPLES AND METHODS

### Mineral name and type materials

The mineral and mineral name (rubinite) have been approved by the Commission on New Minerals, Nomenclature and Classification (CNMNC) of the International Mineralogical Association (IMA 2016-110) (Ma et al. 2017b). The name is in honor of Alan E. Rubin (b. 1953), a cosmochemist at University of California, Los Angeles (UCLA), USA, for his many contributions to research in cosmochemistry and mineralogy of meteorites (e.g., Rubin 1997; Rubin and Ma 2017, 2021).

The type material in Vigarano section VCM3 from Caltech is deposited in the Smithsonian Institution's National Museum of Natural History, Washington DC, USA, under catalogue USNM 7927. The type material in Allende section AE01 is in the Meteorite Collection of Department of Earth Science, Graduate School of Science, Tohoku University, Sendai, Japan. Efremovka sections E101 and E105 are at the University of Hawai‘i at Mānoa, Honolulu, USA, and E40E is in the Vernadsky Institute, Moscow, Russia. The sizes and mineralogy of the rubinite-bearing refractory inclusions are listed in Table 2.

### Analytical techniques

Back-scatter electron (BSE) imaging of rubinite and associated phases in Vigarano and Efremovka was performed using a ZEISS 1550VP field emission SEM. Chemical analyses were carried out at Caltech using a JEOL 8200 electron microprobe interfaced with the Probe for EPMA program from Probe Software, Inc. and operated in focused beam mode at 10 kV and 5 nA or 15 kV and 15 nA with counting times of 20 s on peak and the MAN background method (Donovan and Tingle 1996). Standards were anorthite (Si*K*α, Al*K*α, Ca*K*α), $TiO_2$ (Ti*K*α), fayalite

(Fe*K*α), $Mn_2SiO_4$ (Mn*K*α), forsterite (Mg*K*α), albite (Na*K*α), $Cr_2O_3$ (Cr*K*α), $V_2O_5$ (V*K*α), $ScPO_4$ (Sc*K*α), zircon (Zr*L*α), and $YPO_4$ (Y*L*α). Quantitative elemental microanalyses were processed with the CITZAF correction procedure (Armstrong 1995).

Petrology and mineralogy of rubinite and associated minerals in Allende were observed by BSE imaging using Hitachi S-3400N SEM and JEOL JSM-7001F FE-SEM at Tohoku University. Semi-quantitative analyses of the Allende CAI minerals were performed using Oxford INCA energy-dispersive spectrometers (EDS) installed on both SEMs, at an accelerating voltage of 15 kV and a beam current of 1.0–1.4 nA. Quantitative X-ray microanalyses of rubinite and associated phases in Allende were performed at Tohoku University using JEOL JXA-8530F field-emission electron microprobe equipped with four wavelength-dispersive X-ray spectrometers. A focused electron beam accelerated at 15 kV with a beam current of 10 nA was used to quantify 12 elements, with peak counting times of 10 s for Na; 20 s for Si, Al, Mg and Ca; and 40 s for Ti, Cr, Fe, V, Sc and Y. Standards were diopside (Si*K*α), $TiO_2$ (Ti*K*α), almandine (Al*K*α), $Cr_2O_3$ (Cr*K*α), $Fe_2O_3$ (Fe*K*α), olivine (Mg*K*α), wollastonite (Ca*K*α), albite (Na*K*α), $Ca_3(VO_4)_2$ (V*K*α), cubic zirconia (Zr*L*α, Y*L*α) and $Sc_2O_3$ (Sc*K*α). The rest of analytical conditions followed those used at Caltech. Analytical results are given in Table 3.

Electron back-scatter diffraction analyses of rubinite and associated phases in Vigarano and Efremovka were performed on vibropolished thin sections using methods described in Ma and Rossman (2008a, 2009a). An HKL (now Oxford) EBSD system installed on the Zeiss 1550VP field-emission SEM was operated at 20 kV and 6 nA using a focused beam with a 70° tilted stage and in variable pressure (25 Pa) mode. This approach is designed to allow the study of uncoated samples. The EBSD system was calibrated using a single-crystal silicon standard. The structure of rubinite was determined and cell constants obtained by matching the experimental EBSD patterns with the structures of synthetic $Ca_3Ti^{3+}{}_2Si_3O_{12}$ and other garnet phases (e.g., Valldor et al. 2011). Orientations and identities of other phases were also determined using EBSD. Micro-Raman analysis was carried out with a Renishaw inVia™ Qontor Raman microscope using a green (514 nm) laser at ~0.7 mW power.

EBSD analysis of rubinite and other refractory phases in Allende was performed using Oxford AZtec EBSD system on JEOL JXA-8530F FE-EPMA at Tohoku University, following methods described in Yoshizaki et al. (2019). The surface of the sample was chemically polished by 0.05 μm colloidal silica using BUEHLER VibroMet 2 vibratory polisher for 3 hours, and then coated with a thin layer of carbon. The EBSD analysis was conducted at an acceleration voltage of 20 kV and beam current of 6 nA in focused beam mode with a 70º tilted stage under a high vacuum. A single-crystal silicon standard was used to calibrate the EBSD system.

Oxygen-isotope compositions of rubinite, perovskite, clinopyroxene, spinel, melilite, and olivine in rubinite-bearing inclusions were measured using the University of Hawai‘i (UH) Cameca ims-1280 secondary ion mass-spectrometer (SIMS or ion microprobe). A 15−20 pA focused $Cs^+$ primary ion beam of 20 keV impact energy and ~ 2 μm in diameter was used for SIMS analyses. The secondary ion mass spectrometer was operated at –10 keV with a 40 eV energy window. $^{16}O^-$ and $^{18}O^-$ were measured on a multicollector Faraday cup and electron multiplier (EM), respectively. $^{17}O^-$ was measured with the axial EM. The mass resolving power (m/Δm) for $^{16}O^-$ and $^{18}O^-$ was ~2000, and that for $^{17}O^-$ was ~5500, sufficient for separating contributions from interfering $^{16}OH^-$. A normal-incidence electron flood gun was used for charge compensation. To verify positions of the sputtered regions, spots analyzed for oxygen isotopes were studied with secondary and BSE images using the UH JEOL JXA-8500F electron microprobe before and after SIMS measurements.

Oxygen-isotope compositions are reported in Table 4 as $\delta^{17}O$ and $\delta^{18}O$, deviations from Vienna Standard Mean Ocean Water (VSMOW; $^{17}O/^{16}O_{VSMOW} = 0.000380$; $^{18}O/^{16}O_{VSMOW} = 0.002005$; De Laeter et al. 2003) in parts per thousand: $\delta^{17,18}O_{SMOW} = [(^{17,18}O/^{16}O_{sample}) / (^{17,18}O/^{16}O_{VSMOW}) - 1] \times 1000$, and as deviation from the terrestrial fractionation line, $\Delta^{17}O$ (= $\delta^{17}O - 0.52\times\delta^{18}O$). Instrumental mass fractionation (IMF) was corrected using terrestrial Burma spinel (for perovskite, rubinite), augite (for davisite, Al-diopside), and San Carlos olivine (for forsterite) standards. Since no proper standards exist for the chemically unusual minerals in ultra-refractory CAIs, it is impossible to properly correct for IMF; therefore, only the reported $\Delta^{17}O$

values should be regarded as reliable as the IMF is mass-dependent. The reported 2σ uncertainties include both the internal measurement precision on an individual analysis and the external reproducibility for measurements on standards observed during a given analytical session. The external reproducibility on the multiple analyses of the standard was ~ 1.5−2.5‰ (2σ) for both $\delta^{17}O$ and $\delta^{18}O$.

## RESULTS

### Occurrence

Rubinite is observed in three CV3 carbonaceous chondrites (Table 1). The Vigarano meteorite, which fell near Vigarano Pieve in the province of Ferrara, Italy, on January 22, 1910, is a CV3.1−3.4 chondrite breccia containing the oxidized and reduced lithologies (Krot et al. 2000; Bonal et al. 2006). The Allende meteorite, which fell in and near Pueblito de Allende, Chihuahua, Mexico on February 8, 1969, is a CV>3.6 chondrite of the oxidized subgroup (Clarke et al. 1971). Rubinite was also observed in the Efremovka CV3.1−3.4 chondrite of the reduced subgroup, which was found in July 1962 in the Efremovka State Farm, Pavlodar District, Pavlodar Region, Kazakh SSR, Russia (The Meteoritical Bulletin, 1962). The following paragraphs provide a brief description of each rubinite-bearing inclusion; their sizes and mineralogy are summarized in Table 2.

In the Vigarano ultrarefractory CAI cluster *V3* within an amoeboid olivine aggregate, rubinite occurs in the central portion of an ultrarefractory fragment with Zr,Y,Sc-oxide [$(Y,Sc)_2Zr_5O_{13}$] and spinel, and surrounded by davisite-diopside (Fig. 1). Eringaite (Sc-garnet; $Ca_3Sc_2Si_3O_{12}$) was identified in other ultrarefractory fragments (Ma 2012).

In the Allende Type A CAI *AE01-01* (Fig. 2), rubinite occurs in gehlenitic melilite with nearby perovskite. Other minerals include primary spinel, hibonite, grossite, davisite, grossmanite, and diopside, and secondary anorthite, grossular, Na-melilite, andradite, and hedenbergite. In the Efremovka Compact Type A (CTA) CAIs *E101* and *E105*, rubinite occurs within gehlenitic melilite with perovskite or grossmanite. In the Efremovka UR CAI *40E-1* (Fig. 3), rubinite is observed within gehlenitic melilite with perovskite and overgrows grossmanite.

In the large Efremovka and Allende CAIs, rubinite occurs in spinel-poor regions. In the small Vigarano CAI, rubinite is in contact with spinel.

**Appearance, physical and optical properties**

Rubinite occurs as irregular to subhedral grains, ~0.5−1 μm in size in Vigarano (Fig. 1), 1−8 μm in size in Allende (Fig. 2), 2−25 μm in size in Efremovka (Fig. 3). Rubinite in Efremovka has a bluish brown color. Luster, streak, hardness, tenacity, cleavage, fracture, density, and optical properties could not be determined because of the small grain size. The blue color reflects high concentrations of tri- and quadrivalent Ti. The intensity of blue color of synthetic hibonite has been shown to be associated with increasing $Ti^{3+}$ concentration (Ihinger and Stolper 1986). The blue color of hibonite in the Murchison, Murray and Vigarano meteorites is assigned to $Ti^{3+}$-$Ti^{4+}$ intervalence charge transfer based on the half-width of the absorption (http://minerals.gps.caltech.edu/FILES/Visible/Hibonite/ Index.html). From the empirical formula for the type crystals (Table 3) and the crystal structure, as described below, the densities of rubinite are 4.08 g/cm$^3$ in Vigarano, 3.63 g/cm$^3$ in Allende. Computed densities for rubinite from the three Efremovka occurrences range from 3.11–3.17 g/cm$^3$.

**Chemistry and crystallography**

The mean chemical compositions of rubinite in five meteoritic inclusions obtained by EPMA are given in Table 3.

Vigarano rubinite is Y-, Sc-, and Zr-enriched. Its empirical formula (based on 12 O atoms *pfu*) is $(Ca_{1.89}Y_{0.83}Mg_{0.28})(Ti^{3+}_{0.53}Sc_{0.50}Zr_{0.72}Mg_{0.20}Fe_{0.06}V_{0.02}Cr_{0.01})(Si_{1.64}Al_{1.18}Ti^{4+}_{0.07}Ti_{0.06})O_{12}$, with $Ti^{3+}$ and $Ti^{4+}$ partitioned, based on stoichiometry (8 cations per 12 oxygens). The general formula is $(Ca,Y)_3(Ti^{3+},Sc,Zr)_2(Si,Al)_3O_{12}$.

The empirical formula (based on 12 O atoms *pfu*) of Allende rubinite is $(Ca_{2.94}Na_{0.08})(Ti^{3+}_{1.04}Ti^{4+}_{0.59}Sc_{0.13}Mg_{0.10}V_{0.04}Fe_{0.04}Zr_{0.03})(Si_{2.38}Al_{0.38}Ti^{4+}_{0.24})O_{12}$, with $Ti^{3+}$ and $Ti^{4+}$ partitioned, based on stoichiometry. Its general formula is $Ca_3(Ti^{3+},Ti^{4+},Sc)_2(Si,Al,Ti^{4+})_3O_{12}$.

DOI: https://doi.org/10.2138/am-2024-9435. http://www.minsocam.org/

The empirical formulae of Efremovka rubinite are $(Ca_{3.03}Na_{0.03})(Ti^{3+}_{1.04}Ti^{4+}_{0.64}Mg_{0.11}Al_{0.06}Sc_{0.04}V_{0.04}Zr_{0.01})(Si_{2.54}Al_{0.46})O_{12}$ in *E101*, $(Ca_{3.00}Na_{0.03})(Ti^{3+}_{1.06}Ti^{4+}_{0.66}Mg_{0.10}Sc_{0.08}V_{0.04}Fe_{0.01}Zr_{0.01})(Si_{2.39}Al_{0.49}Ti^{4+}_{0.12})O_{12}$ in *E105*, and $(Ca_{2.98}Na_{0.03})(Ti^{3+}_{1.06}Ti^{4+}_{0.60}Mg_{0.13}Sc_{0.11}Zr_{0.05}V_{0.02}Fe_{0.01})(Si_{2.25}Al_{0.48}Ti^{4+}_{0.27})O_{12}$ in *40E-1*, with $Ti^{3+}$ and $Ti^{4+}$ partitioned, based on stoichiometry. The general formula is $Ca_3(Ti^{3+},Ti^{4+},Mg)_2(Si,Al)_3O_{12}$ or $Ca_3(Ti^{3+},Ti^{4+},Mg,Sc)_2(Si,Al,Ti^{4+})_3O_{12}$.

According to the valence dominant rule (Hatert and Burke 2008) and the newly-approved nomenclature on the garnet supergroup (Grew et al. 2013), this $Ti^{3+}$-rich silicate is a new garnet group mineral. It end-member formula is $Ca_3Ti^{3+}_2Si_3O_{12}$, which requires $SiO_2$ 36.62, $Ti_2O_3$ 29.21, CaO 34.17, total 100.00 wt%.

EBSD patterns of rubinite obtained in all five occurrences match the structure of synthetic $Ca_3Ti^{3+}_2Si_3O_{12}$ from Valldor et al. (2011) with mean angular deviations ranging from 0.1º to 0.5º (Fig. 4). Rubinite is cubic with space group $Ia\bar{3}d$ and has cell parameters $a$ = 12.19(1) Å, $V$ = 1811(4) Å$^3$, and $Z$ = 8.

The Raman spectrum of rubinite shows numerous features under the green laser. Prominent ones are at 870, 847, 792, 598, 546, 513, 485, 354, and 336 cm$^{-1}$ (Fig. 5).

**Coexisting phases**

A general mineralogical theme of rubinite-bearing inclusions is one of exclusion (Table 2). Vigarano UR *V3* has abundant Zr,Y,Sc-oxide but no perovskite and no melilite. The four rubinite-bearing inclusions in Allende and Efremovka have perovskite and melilite with no Zr,Y,Sc-oxide. Eringaite was observed only in *AE01-01* and *V3*, hibonite only in *AE01-01*.

In UR *V3*, Vigarano rubinite is very Y-, Sc-, and Zr-rich. Associated Zr,Y,Sc-oxide has an empirical formula of $(Y_{0.64}Sc_{0.59}Ti_{0.37}Ca_{0.29}Mg_{0.07}Fe_{0.06}Al_{0.04})(Zr_{4.82}Hf_{0.09}Si_{0.05})O_{13}$, showing a general formula of $(Y,Sc)_2Zr_5O_{13}$. Eringaite is a Sc-rich garnet, occurring in other UR fragments with an empirical formula of $(Ca_{2.31}Y_{0.57}Mg_{0.12})(Sc_{0.82}Ti^{3+}_{0.32}Mg_{0.44}Ti^{4+}_{0.25}Zr_{0.10}Fe_{0.05}V_{0.03}Cr_{0.01})(Si_{2.47}Al_{0.44}Ti^{4+}_{0.09})O_{12}$ (Ma 2012).

In Allende *AE01-01*, rubinite-hosting melilite ($Åk_{11}$) has an empirical formula of $Ca_{2.03}(Al_{0.86}Mg_{0.12})(Si_{1.11}Al_{0.89})O_7$. Nearby perovskite is $Ca_{1.01}(Ti_{0.98}Si_{0.01}Al_{0.01})O_3$. Hibonite has an empirical formula of $Ca_{1.02}(Al_{10.85}Mg_{0.57}Ti^{3+}_{0.52}Si_{0.03}Cr_{0.01})O_{19}$.

In the three Efremovka CAIs, melilite ($Åk_{13}$) has similar compositions with an empirical formula of ~$Ca_{2.04}(Al_{0.84}Mg_{0.13})(Si_{1.13}Al_{0.87})O_7$. Associated perovskite is ~$Ca_{1.00}(Ti_{0.98}Al_{0.01})O_3$. In CAI *40E-1*, rubinite overgrows grossmanite (Fig. 3c).

**Oxygen isotopes**

Oxygen-isotope compositions of rubinite-bearing CAIs are listed in Table 4 and depicted in Figure 6. Since rubinite was not measured in *V3*, data for minerals coexisting with rubinite in this CAI are only listed in Table 4. All of the isotopic compositions plot below the terrestrial fractionation line and lie approximately along a slope-1 line. However, because most minerals were measured without proper standards (see above), it is not possible to properly correct the instrumental fractionation effects. Therefore, only $\Delta^{17}O$ values are discussed below. All rubinite-bearing CAIs measured have heterogeneous $\Delta^{17}O$. In the Efremovka CAIs *E101*, *E105*, and *40E*, spinel, perovskite, and most rubinite grains have $^{16}O$-rich compositions ($\Delta^{17}O$ range from ~ −25 to ~ −20‰); melilite and Ti-rich pyroxenes are $^{16}O$-depleted ($\Delta^{17}O$ range from ~ −10 to ~ −5‰). In the Allende CTA *AE01-01*, spinel and hibonite are $^{16}O$-rich ($\Delta^{17}O$ ~ –24‰); melilite, rubinite and perovskite show large ranges in $\Delta^{17}O$ (from –23 to –3‰, from –21 to –6‰, and from –14 to –2‰, respectively); grossmanite is uniformly $^{16}O$-depleted ($\Delta^{17}O$ ~ –3‰).

## DISCUSSION

Rubinite, $Ca_3Ti^{3+}_2Si_3O_{12}$, is a new member of the garnet group and the $Ti^{3+}$-analog of eringaite $Ca_3Sc_2Si_3O_{12}$, grossular $Ca_3Al_2Si_3O_{12}$, goldmanite $Ca_3V_2Si_3O_{12}$, uvarovite $Ca_3Cr_2Si_3O_{12}$, or andradite $Ca_3Fe_2Si_3O_{12}$. Like meteoritic eringaite, rubinite formed either as a gas-solid condensate or through crystallization from an $^{16}O$-rich Ca, Al, and Ti-rich melt under highly reducing, solar-like conditions.

Texturally, rubinite, Zr,Y,Sc-oxide and spinel formed early in the Vigarano ultrarefractory inclusion *V3* before the appearance of davisite and Sc-rich diopside. Forsterite condensed around the refractory inclusion at a later stage in the nebula. In the Allende and Efremovka Type A CAIs, rubinute typically encloses perovskite, and is either overgrown by grossmanite or overgrows it.

All rubinite-bearing igneous CAIs studied have internally heterogeneous O-isotope compositions, suggesting either crystallization from a melt that experienced O-isotope exchange with a nebular gas with variable $\Delta^{17}O$ (e.g., Yurimoto et al. 1998; Kawasaki et al. 2018) or postcrystallization O-isotope exchange with an $^{16}O$-depleted external reservoir: either nebular gas or aqueous fluid on the CV parent asteroid (Krot et al. 2022). Because CAIs from unmetamorphosed carbonaceous chondrites (CI, CM, CR, CO) of petrologic type ≤3.0 have internally uniform solar-like $^{16}O$-rich compositions ($\Delta^{17}O \sim -24\pm2$‰), whereas CAIs from meteorites of petrologic type > 3.0 which experienced fluid-assisted thermal metamorphism/metasomatic alteration (CV, CO, CK) are isotopically heterogeneous (Krot et al. 2021, 2022 and references therein), O-isotope exchange on the CV parent asteroid seems likely. This is also consistent with our observations that rubinite in less altered and the less metamorphosed chondrite Efremovka ($CV_{red}$3.1–3.4) appears to have largely preserved the initial $^{16}O$-rich solar-like composition, whereas rubinite in the extensively altered and more metamorphosed chondrite Allende ($CV_{ox}$>3.6) is significantly $^{16}O$-depleted (Fig. 6). The $\Delta^{17}O$ values of the most $^{16}O$-depleted rubinite grains approach $\Delta^{17}O$ of the Allende aqueous fluid, $-3\pm2$‰, inferred from O-isotope composition of secondary minerals in the Allende CAIs (Krot et al. 2022). We note, however, that O-isotope self-diffusion in CAI minerals, including $Ti^{3+}$-rich garnet rubinite and $Ti^{3+}$-rich grossmanite, under metasomatic alteration conditions experienced by CV chondrites are not known. Therefore, the exact mechanism of O-isotope heterogeneity in CV CAIs remains unclear. For arguments in favor or against O-isotope exchange in the solar nebula vs. O-isotope exchange with aqueous fluid on chondrite parent asteroids, see Krot et al. (2022).

## IMPLICATIONS

Rubinite is among other 50+ refractory minerals identified in carbonaceous chondrites (Rubin and Ma 2021), which mark the beginning of mineral evolution in the solar system. Meteorite garnets found predominantly in CV CAIs appear to have recorded *p*-*T*-$fO_2$ conditions and O-isotope compositions in the solar nebular and in the CV asteroidal body. Rubinite ($Ca_3Ti^{3+}{}_2Si_3O_{12}$) and eringaite ($Ca_3Sc_2Si_3O_{12}$) are high-temperature primary garnets formed either by gas-solid condensation and/or igneous crystallization under highly reducing conditions in the solar nebula. Grossular ($Ca_3Al_2Si_3O_{12}$), andradite ($Ca_3Fe^{3+}{}_2Si_3O_{12}$), and hutcheonite [$Ca_3Ti^{4+}{}_2(SiAl_2)O_{12}$] are low-temperature secondary garnets formed under oxidizing conditions during metasomatic alteration on the CV parent asteroid (Krot et al. 2021).

## ACKNOWLEDGEMENTS

SEM, EBSD and EPMA analyses were carried out at the Caltech GPS Division Analytical Facility, which is supported, in part, by NSF Grants EAR-0318518 and DMR-0080065. We appreciate Issei Narita and Yoshinori Ito for technical assistance for EPMA analyses at Tohoku University, and Makoto Kimura for providing EPMA standard materials. The meteorite sections studied are from Caltech, Tohoku University, University of Hawaiʻi at Manoa, and the Vernadsky Institute. Marina A. TY acknowledges supports from the Japanese Society for the Promotion of Science (JP18J20708), GP-EES Research Grant and DIARE Research Grant. MAI acknowledges the support from the Vernadsky Institute. SIMS measurements were supported by NASA grant 80NSSC23K0253 (PI A.N. Krot). We thank Jessica Johnson, an anonymous reviewer and Associate Editor Steven B. Simon for their constructive reviews on the manuscript.

## REFERENCES

Armstrong, J.T. (1995) CITZAF: A package of correction programs for the quantitative electron beam X-ray analysis of thick polished materials, thin films, and particles. Microbeam Analysis, 4, 177–200.

Bonal, L., Bourot-Denise, M., Quirico, E. and Montagnac, G. (2006) Determination of the petrologic type of CV3 chondrites by Raman spectroscopy of included organic matter. Geochimica et Cosmochimica Acta, 70, 1849−1863.

Borriello, R., Xiong, F., Ma, C., Lorenzon, S., Mugnaioli, E., Yang, J., Xu, X. and Grew, E.S. (2024) Jianmuite, $ZrTi^{4+}Ti^{3+}{}_5Al_3O_{16}$, a new mineral from the Allende meteorite and from chromitite near Kangjinla, Tibet, China. American Mineralogist, revision submitted.

Clarke, R.S., Jr., Jarosewich, E., Mason, B., Nelen, J., Gomez, M. and Hyde, J.R. (1971) Allende, Mexico, Meteorite Shower. Smithsonian Contributions to the Earth Sciences, 5, 1–53.

De Laeter, J.R., Bohlke, J.K., De Bièvre, P., Hidaka, H., Peiser, H.S., Rosman, K.J.R. and Taylor, P.D.P. (2003) Atomic Weights of the Elements: Review 2000 (IUPAC Technical Report). Pure and Applied Chemistry, 75: 683–800.

Fuchs, L. (1971) Occurrence of wollastonite, rhönite, and andradite in the Allende meteorite. American Mineralogist, 56, 2053−2068.

Fuchs, L. (1978) The mineralogy of a rhönite-bearing calcium aluminum rich inclusion in the Allende meteorite. Meteoritics, 13, 73−88.

Grew, E.S., Locock, A.J., Mills, S.J., Galuskina, I.O., Galuskin, E.V. and Hålenius, U. (2013) Nomenclature of the garnet supergroup. American Mineralogist, 98, 785–811.

Hatert, F. and Burke, E.A.J. (2008) The IMA-CNMNC dominant-constituent rule revisited and extended. Canadian Mineralogist, 46, 717–728.

Ihinger, P.D. and Stolper, E.M. (1986) The color of meteoritic hibonite: an indicator of oxygen fugacity. Earth and Planetary Science Letters, 78, 67–79.

Ivanova, M.A., Krot, A.N., Nagashima, K., Ma, C. and MacPherson G.J. (2017) Oxygen-isotope composition of ultrarefractory CAI from CV3 chondrite. Meteoritics & Planetary Science, 52 (S1). Abstract No 6037.

Kawasaki, N., Simon, S.B., Grossman, L., Sakamoto, N., and Yurimoto, H. (2018) Crystal growth and disequilibrium distribution of oxygen isotopes in an igneous Ca-Al-rich inclusion from the Allende carbonaceous chondrite. Geochimica et Cosmochimica Acta, 221, 318–341.

Krot, A.N., Meibom, A., and Keil, K. (2000) A clast of Bali-like oxidized CV3 material in the reduced CV3 chondrite breccia Vigarano. Meteoritics & Planetary Science, 35, 817−827.

Krot, A.N., Ma, C., Nagashima, K., Davis, A.M., Beckett, J.R., Simon, S.B., Komatsu, M., Fagan, T.J., Brenker, F., Ivanova, M.A. and Bischoff, A. (2019) Mineralogy, petrography, and oxygen isotopic compositions of ultrarefractory inclusions from carbonaceous chondrites. Chemie der Erde - Geochemistry, 79, 125519.

Krot, A.N., Nagashima, K. and Rossman, G.R. (2020) Machiite, $Al_2Ti_3O_9$, a new oxide mineral from the Murchison carbonaceous chondrite: A new ultra-refractory phase from the solar nebula. American Mineralogist, 105, 239–243.

Krot, A.N., Petaev, M.I., and Nagashima, K. (2021) Infiltration metasomatism of the Allende coarse-grained calcium-aluminum-rich inclusions. Progress in Earth and Planetary Science, 8, 61.

Krot A.N., Nagashima, K., MacPherson, G.J., and Ulyanov, A.A. (2022) On the nature of oxygen-isotope heterogeneity of igneous calcium-aluminum-rich inclusions in CV carbonaceous chondrites. Geochimica et Cosmochimica Acta, 332, 327–354.

Ma, C. (2010) Hibonite-(Fe), $(Fe,Mg)Al_{12}O_{19}$, a new alteration mineral from the Allende meteorite. American Mineralogist, 95, 188–191.

Ma, C. (2012) Discovery of meteoritic eringaite, $Ca_3(Sc,Y,Ti)_2Si_3O_{12}$, the first solar garnet? Meteoritics & Planetary Science, 47 (S1), A256.

Ma, C. (2018) Discovery of meteoritic baghdadite, $Ca_3(Zr,Ti)Si_2O_9$, in Allende: The first solar silicate with structurally essential zirconium? Meteoritics and Planetary Science, 53 (S1), Abstract No. 6358.

Ma, C. (2020) Discovery of meteoritic calzirtite in Leoville: A new ultrarefractory phase from the solar nebula. Goldschmidt 2020, Abstract No. 1674. DOI:10.46427/gold2020.1674

Ma, C. and Beckett, J.R. (2021) Kaitianite, $Ti^{3+}{}_2Ti^{4+}O_5$, a new titanium oxide mineral from Allende. Meteoritics & Planetary Science, 56, 96–107.

Ma, C. and Krot, A.N. (2014) Hutcheonite, $Ca_3Ti_2(SiAl_2)O_{12}$, a new garnet mineral from the Allende meteorite: An alteration phase in a Ca-Al-rich inclusion. American Mineralogist, 99, 667–670.

Ma, C. and Rossman, G.R. (2008a) Barioperovskite, $BaTiO_3$, a new mineral from the Benitoite Mine, California. American Mineralogist, 93, 154–157.

Ma, C. and Rossman, G.R. (2008b) Discovery of tazheranite (cubic zirconia) in the Allende meteorite. Geochimica et Cosmochimica Acta, 72, 12S, A577.

Ma, C. and Rossman, G.R. (2009a) Davisite, $CaScAlSiO_6$, a new pyroxene from the Allende meteorite. American Mineralogist, 94, 845–848.

Ma, C. and Rossman, G.R. (2009b) Grossmanite, $CaTi^{3+}AlSiO_6$, a new pyroxene from the Allende meteorite. American Mineralogist, 94, 1491–1494.

Ma, C. and Rossman, G.R. (2009c) Tistarite, $Ti_2O_3$, a new refractory mineral from the Allende meteorite. American Mineralogist, 94, 841–844.

Ma, C., Tschauner, O., Beckett, J.R., Rossman, G. and Liu, W. (2012) Panguite, $(Ti^{4+},Sc,Al,Mg,Zr,Ca)_{1.8}O_3$, a new ultra-refractory titania mineral from the Allende meteorite: Synchrotron micro-diffraction and EBSD. American Mineralogist, 97, 1219–1225.

Ma, C., Beckett, J.R., Connolly, Jr H.C. and Rossman, G.R. (2013a) Discovery of meteoritic loveringite, $Ca(Ti,Fe,Cr,Mg)_{21}O_{38}$, in an Allende chondrule: Late-stage crystallization in a melt droplet. 44th Lunar and Planetary Science Conference, Abstract # 1443.

Ma, C., Tschauner, O., Beckett, J.R., Rossman, G. and Liu, W. (2013b) Kangite, $(Sc,Ti,Al,Zr,Mg,Ca,[])_2O_3$, a new ultrarefractory scandia mineral from the Allende meteorite: Synchrotron micro-Laue diffraction and electron backscatter diffraction. American Mineralogist, 98, 870–878.

Ma, C., Krot, A.N. and Nagashima, K. (2017a) Addibischoffite, $Ca_2Al_6Al_6O_{20}$, a new calcium aluminate mineral from the Acfer 214 CH carbonaceous chondrite: A new refractory phase from the solar nebula. American Mineralogist, 102, 1556−1560.

Ma, C., Yoshizaki, T., Nakamura, T. and Muto, J. (2017b) Rubinite, IMA 2016-110. CNMNC Newsletter No. 36, April 2017, page 408. Mineralogical Magazine, 81, 403–409.

Ma, C., Yoshizaki, T., Krot, A.N., Beckett, J.R., Nakamura, T., Nagashima, K., Muto, J. and Ivanova, M.A. (2017c) Discovery of rubinite, $Ca_3Ti^{3+}{}_2Si_3O_{12}$, a new garnet mineral in refractory inclusions from carbonaceous chondrites. Meteoritics & Planetary Science, 52 (S1), Abstract No. 6023.

Ma, C., Krot, A.N., Beckett, J.R., Nagashima, K., Tschauner, O., Rossman, G.R., Simon, S.B. and Bischoff, A. (2020) Warkite, $Ca_2Sc_6Al_6O_{20}$, a new mineral in carbonaceous chondrites and a key-stone phase in ultrarefractory inclusions from the solar nebula. Geochimica et Cosmochimica Acta, 277, 52–86.

Ma, C., Krot, A.N., Paque, J.M., Tschauner, O. and Nagashima, K. (2021) Beckettite, $Ca_2V_6Al_6O_{20}$, a new mineral in a Type A refractory inclusion from Allende and clues to processes in the early solar system. Meteoritics & Planetary Science, 56, 2265–2272.

Ma, C., Beckett, J.R., Tissot F.L.H. and Rossman, G.R. (2022) New minerals in type A inclusions from Allende and clues to processes in the early solar system: Paqueite, $Ca_3TiSi_2(Al,Ti,Si)_3O_{14}$, and burnettite, $CaVAlSiO_6$. Meteoritics & Planetary Science, 57, 1300–1324.

Ma, C., Borriello, R., Xiong, F., Lorenzon, S., Mugnaioli, E., Yang, J., Xu, X., and Grew, E. S. (2024a) Discovery of new nineral jianmuite, $ZrTi^{4+}Ti^{3+}{}_5Al_3O_{16}$, in the Allende meteorite: An ultrarefractory phase from the solar nebula. Meteoritics & Planetary Science, 59 (S1), Abstract 6039.

Ma, C., Krot, A,N., Nagashima, K. and Dunn, T. (2024b) Louisfuchsite, $Ca_2(Mg_4Ti_2)(Al_4Si_2)O_{20}$, a new rhönite-type mineral from the NWA 4964 CK meteorite: A refractory phase from the solar nebula. American Mineralogist, early publication. https://doi.org/10.2138/am-2023-9283

McKeegan K. D., Kallio A. P. A., Heber V. S., Jarzebinski G., Mao P. H., Coath C. D., Kunihiro T., Wiens R. C., Nordholt J. E., Moses R. W., Jr., Reisenfeld D. B., Jurewicz A. J. G., and Burnett D. S. (2011) The oxygen isotopic composition of the Sun inferred from captured solar wind. Science, 332, 1528–1532.

Rubin, A.E. (1997) Mineralogy of meteorite groups. Meteoritics & Planetary Science, 32, 231–247.

Rubin, A.E. and Ma, C. (2017) Meteoritic minerals and their origins. Chemie der Erde - Geochemistry, 77, 325–385.

Rubin, A.E. and Ma, C. (2021) Meteorite Mineralogy. Cambridge Planetary Science (26). Cambridge University Press. DOI:10.1017/9781108613767

Valldor, M., Uthe, A. and Ruckamp, R. (2011) Antiferromagnetic ground state of quantum spins in the synthetic imanite, $Ca_3Ti_2Si_3O_{12}$: The lost child of the garnet family. Inorganic Chemistry, 50, 10107–10112.

Yoshizaki, T., Nakashima, D., Nakamura, T., Park, C., Sakamoto, N., Ishida, H., and Itoh, S. (2019) Nebular history of an ultrarefractory phase bearing CAI from a reduced type CV chondrite. Geochimica et Cosmochimica Acta, 252, 39–60.

Yurimoto H., Krot A. N., Choi B.-G., Aléon J., Kunihiro T., and Brearley A. J. (2008) Oxygen isotopes of chondritic components. In Oxygen in the Solar System (ed. MacPherson G. J.), Reviews in Mineralogy & Geochemistry, 68, 141−187.

Xiong, Y., Zhang, A.-C., Kawasaki, N., Ma, C., Sakamoto, N., Chen, J.-N., Gu, L.-X. and Yurimoto, H. (2020) Mineralogical and oxygen isotopic study of a new ultrarefractory inclusion in the Northwest Africa 3118 CV3 chondrite. Meteoritics & Planetary Science, 55, 2164–2205.

**Table 1.** Refractory and secondary Ti-rich minerals identified in carbonaceous chondrites.

| Mineral | Formula | Reference |
|---|---|---|
| *Primary refractory phases* | | |
| addibischoffite | $Ca_2(Al,Mg,V,Ti)_6(Al,Si)_6O_{20}$ | Ma et al. (2017a) |
| Al,Ti-diopside (fassaite) | $Ca(Mg,Ti,Al)(Si,Al)_2O_6$ | Clarke et al. (1971) |
| baghdadite | $Ca_3(Zr,Ti)Si_2O_9$ | Ma (2018) |
| beckettite | $Ca_2(V,Al,Ti,Al,Mg)_6Al_6O_{20}$ | Ma et al. (2021) |
| burnettite | $Ca(V,Sc,Ti,Al,Mg)AlSiO_6$ | Ma et al. (2022) |
| calzirtite | $Ca_2Zr_5Ti_2O_{16}$ | Ma (2020), Xiong et al. (2020) |
| davisite | $Ca(Sc,Ti^{3+},Al,Mg)AlSiO_6$ | Ma and Rossman (2009a) |
| eringaite | $Ca_3(Sc,Ti^{3+})_2Si_3O_{12}$ | Ma (2012), Ma et al. (2020) |
| grossmanite | $Ca(Ti^{3+},Sc,Al,Mg)AlSiO_6$ | Ma and Rossman (2009b) |
| jianmuite | $ZrTi^{4+}Ti^{3+}{}_5Al_3O_{16}$ | Ma et al. (2024a), Borriello et al. (2024) |
| kaitianite | $Ti^{3+}{}_2Ti^{4+}O_5$ | Ma and Beckett (2021) |
| kangite | $(Sc,Ti^{4+},Al,Zr,Mg,Ca)_{1.8}O_3$ | Ma et al. (2013b) |
| khmrabaevite | TiC | Ma and Rossman (2009c) |
| louisfuchsite (rhonite) | $Ca_2(Mg_4Ti_2)(Al_4Si_2)O_{20}$ | Fuchs (1971, 1978), Ma et al. (2024b) |
| machiite | $(Al,Sc)_2(Ti,Zr)_3O_9$ | Krot et al. (2020) |
| mullite | $(Al,Ti^{3+})_6Si_2O_{13}$ | Ma and Beckett (2021) |
| osbornite | TiN | Ma and Beckett (2021) |
| panguite | $(Ti^{4+},Al,Sc,Mg,Zr,Ca)_{1.8}O_3$ | Ma et al. (2012) |
| paqueite | $Ca_3TiSi_2(Al_2Ti)O_{14}$ | Ma et al. (2022) |
| perovskite | $CaTiO_3$ | Clarke et al. (1971) |
| rubinite | $Ca_3Ti^{3+}{}_2Si_3O_{12}$ | Ma et al. (2017c), this study |
| rutile | $TiO_2$ | Ma and Rossman (2009c) |
| tazheranite | $(Zr,Ti^{4+},Sc,Y,Ca)O_{1.75}$ | Ma and Rossman (2008b) |
| tistarite | $Ti_2O_3$ | Ma and Rossman (2009c) |
| sassite (anosovite) | $(Ti^{4+},Ti^{3+},Mg,Sc,Al)_3O_5$ | Zhang et al. (2015) |
| warkite | $Ca_2(Sc,Ti,Al,Mg,Zr)_6Al_6O_{20}$ | Ma et al. (2020) |
| zirconolite | $CaZrTi_2O_7$ | Ma and Rossman (2008b) |
| zirkelite | $(Ti^{4+},Zr,Sc,Y,Ca)O_{1.75}$ | Krot et al. (2019) |
| *Secondary phases* | | |
| ilmenite | $FeTiO_3$ | Ma (2010) |
| hutcheonite | $Ca_3Ti^{4+}{}_2(SiAl_2)O_{12}$ | Ma and Krot (2014) |
| loveringite | $Ca(Ti,Fe,Cr,Mg)_{21}O_{38}$ | Ma et al. (2013a) |

**Table 2.** Mineralogy of rubinite-bearing CAIs in carbonaceous chondrites.

| Chondrite | Vigarano | Allende | Efremovka | Efremovka | Efremovka |
|---|---|---|---|---|---|
| type | CV3.2–3.4 | CV>3.6 | CV3.1–3.4 | CV3.1–3.4 | CV3.1–3.4 |
| section # | VCM3 | AE01 | E101 | E105 | 40E |
| collection | Caltech | Tohoku U. | Hawaiʻi U. | Hawaiʻi U. | Vernadsky Inst. |
| CAI | *V3* | *AE01-01* | *E101* | *E105* | *40E-1* |
| size, μm | 20×30 | 3000×6000 | 3500×4000 | 4000×4500 | 800×1200 |
| rb | + | + | + | + | + |
| ern | + | + | – | – | – |
| ZYS | + | – | – | – | – |
| PGEs | + | – | – | – | – |
| pv | – | + | + | + | + |
| hib | – | + | – | – | – |
| cor | – | + | – | – | – |
| sp | + | + | + | + | + |
| mel | – | + | + | + | + |
| dav | + | + | – | – | – |
| grs | – | + | – | – | – |
| grm | – | + | + | + | + |
| Al-di | + | + | + | + | + |
| fo | + | – | – | – | – |

Sign "+" means present; sign "–" means absent. Al-di = Al-diopside; cor = corundum; dav = davisite; ern = eringaite; fo = forsterite; grm = grossmanite; grs = grossite; hib = hibonite; mel = melilite; PGEs = platinum group element-rich alloys; pv = perovskite; rb = rubinite; sp = spinel; ZYS = Zr,Y,Sc-oxide.

DOI: https://doi.org/10.2138/am-2024-9435. http://www.minsocam.org/

**Table 3.** EPMA results of rubinite in five CAIs from the CV3 Vigarano, Allende and Efremovka chondrites.

| Constituent wt% | Vigarano *V3* n=3 | SD | Allende *AE01-01* n=3 | SD | Efremovka *E101* n=13 | SD | Efremovka *E105* n=13 | SD | Efremovka *40E* n=23 | SD |
|---|---|---|---|---|---|---|---|---|---|---|
| $SiO_2$ | 17.41 | 0.51 | 28.37 | 0.49 | 31.09 | 1.00 | 28.61 | 0.65 | 27.19 | 0.83 |
| $Ti_2O_3$ | 7.53 | 0.19 | 14.79 | 0.43 | 15.15 | 0.70 | 15.27 | 0.40 | 15.26 | 0.60 |
| $TiO_2$ | 0.96 | 0.02 | 13.06 | 0.50 | 10.39 | 0.48 | 12.45 | 0.33 | 13.96 | 0.55 |
| $Al_2O_3$ | 10.65 | 0.17 | 3.82 | 0.16 | 5.36 | 1.09 | 4.97 | 0.24 | 4.93 | 0.42 |
| $Cr_2O_3$ | 0.09 | 0.04 | 0.05 | 0.02 | n.a. | | n.a. | | n.a. | |
| FeO* | 0.79 | 0.15 | 0.53 | 0.12 | 0.00 | 0.29 | 0.11 | 0.16 | 0.11 | 0.28 |
| MnO | n.a. | | 0.00 | 0.00 | n.a. | | n.a. | | n.a. | |
| MgO | 3.42 | 0.04 | 0.79 | 0.11 | 0.90 | 0.08 | 0.83 | 0.04 | 1.04 | 0.13 |
| CaO | 18.68 | 0.57 | 32.68 | 0.41 | 34.49 | 1.06 | 33.59 | 0.35 | 33.50 | 0.39 |
| $Na_2O$ | n.a. | | 1.01 | 0.04 | 0.19 | | 0.21 | 0.31 | 0.20 | 0.33 |
| $V_2O_3$ | 0.29 | 0.04 | 0.61 | 0.09 | 0.62 | 0.26 | 0.54 | 0.23 | 0.35 | 0.22 |
| $ZrO_2$ | 15.69 | 0.85 | 0.80 | 0.15 | 0.26 | 0.04 | 0.29 | 0.11 | 1.32 | 0.29 |
| $Sc_2O_3$ | 6.13 | 0.07 | 1.80 | 0.35 | 0.62 | 0.43 | 1.08 | 0.50 | 1.50 | 1.12 |
| $Y_2O_3$ | 16.49 | 0.74 | 0.07 | 0.07 | 0.05 | 0.05 | 0.09 | 0.03 | 0.18 | 0.04 |
| Total | 98.13 | | 98.36 | | 99.11 | | 98.03 | | 99.55 | |
| | | | | | | | | | | |
| No. O atoms | 12 | | 12 | | 12 | | 12 | | 12 | |
| Si | 1.64 | | 2.38 | | 2.54 | | 2.39 | | 2.25 | |
| $Ti^{3+}$ | 0.59 | | 1.04 | | 1.04 | | 1.06 | | 1.06 | |
| $Ti^{4+}$ | 0.07 | | 0.83 | | 0.64 | | 0.78 | | 0.87 | |
| Al | 1.18 | | 0.38 | | 0.52 | | 0.49 | | 0.48 | |
| Cr | 0.01 | | 0.00 | | | | | | | |
| Fe | 0.06 | | 0.04 | | 0.00 | | 0.01 | | 0.01 | |
| Mn | | | 0.00 | | | | | | | |
| Mg | 0.48 | | 0.10 | | 0.11 | | 0.10 | | 0.13 | |
| Ca | 1.89 | | 2.94 | | 3.03 | | 3.00 | | 2.98 | |
| Na | | | 0.08 | | 0.03 | | 0.03 | | 0.03 | |
| V | 0.02 | | 0.04 | | 0.04 | | 0.04 | | 0.02 | |
| Zr | 0.72 | | 0.03 | | 0.01 | | 0.01 | | 0.05 | |
| Sc | 0.50 | | 0.13 | | 0.04 | | 0.08 | | 0.11 | |
| Y | 0.83 | | 0.00 | | 0.00 | | 0.00 | | 0.01 | |
| Cation sum | 7.99 | | 8.00 | | 8.00 | | 8.00 | | 8.00 | |

*All Fe is assumed to be $Fe^{2+}$.

467

**Table 4.** Oxygen isotopic compositions of rubinite-bearing CAIs from CV CAIs.

| CAI | mineral | $\delta^{18}O$ | 2σ | $\delta^{17}O$ | 2σ | $\Delta^{17}O$ | 2σ |
|---|---|---|---|---|---|---|---|
| *AE01-01* | | | | | | | |
| -"- | grs | 3.1 | ±0.8 | -1.7 | ±0.6 | -3.3 | ±0.7 |
| -"- | grs | 2.2 | ±0.7 | -1.8 | ±0.6 | -2.9 | ±0.7 |
| -"- | grs | 2.4 | ±0.7 | -1.8 | ±0.5 | -3.1 | ±0.7 |
| -"- | grs | 2.5 | ±0.7 | -1.4 | ±0.6 | -2.7 | ±0.7 |
| -"- | grs | 2.4 | ±0.7 | -2.4 | ±0.5 | -3.7 | ±0.6 |
| -"- | grs | 2.5 | ±0.7 | -2.1 | ±0.5 | -3.4 | ±0.6 |
| -"- | hib | -45.1 | ±0.7 | -47.4 | ±0.8 | -23.9 | ±0.8 |
| -"- | hib | -44.8 | ±0.7 | -46.7 | ±0.7 | -23.4 | ±0.8 |
| -"- | hib | -45.2 | ±0.7 | -47.1 | ±0.6 | -23.6 | ±0.7 |
| -"- | hib | -46.1 | ±0.7 | -47.6 | ±0.6 | -23.6 | ±0.7 |
| -"- | hib | -45.7 | ±0.7 | -47.6 | ±0.7 | -23.9 | ±0.7 |
| -"- | mel | -3.8 | ±0.7 | -6.7 | ±1.9 | -4.7 | ±1.9 |
| -"- | mel | -12.1 | ±0.7 | -15.3 | ±1.9 | -9.0 | ±1.9 |
| -"- | mel | 0.9 | ±0.6 | -2.5 | ±1.9 | -3.0 | ±1.9 |
| -"- | mel | -10.3 | ±0.7 | -13.4 | ±1.9 | -8.0 | ±1.9 |
| -"- | mel | -10.5 | ±0.7 | -14.2 | ±1.9 | -8.7 | ±2.0 |
| -"- | mel | -28.8 | ±0.7 | -31.0 | ±1.9 | -16.1 | ±2.0 |
| -"- | mel | -13.4 | ±0.7 | -16.8 | ±1.9 | -9.8 | ±1.9 |
| -"- | mel | -38.0 | ±0.6 | -39.8 | ±1.9 | -20.1 | ±1.9 |
| -"- | mel | -12.3 | ±1.3 | -15.6 | ±2.2 | -9.2 | ±2.4 |
| -"- | mel | -41.7 | ±0.6 | -43.4 | ±1.9 | -21.6 | ±1.9 |
| -"- | mel | 2.3 | ±0.7 | -2.0 | ±1.9 | -3.1 | ±1.9 |
| -"- | mel | 1.9 | ±0.7 | -2.0 | ±1.9 | -3.0 | ±1.9 |
| -"- | mel | 2.1 | ±0.7 | -1.8 | ±1.9 | -2.9 | ±1.9 |
| -"- | mel | -44.8 | ±0.6 | -45.9 | ±1.9 | -22.6 | ±1.9 |
| -"- | mel | -15.5 | ±0.6 | -18.4 | ±1.9 | -10.3 | ±1.9 |
| -"- | mel | -45.0 | ±0.7 | -45.5 | ±1.9 | -22.1 | ±1.9 |
| -"- | mel | 1.8 | ±0.6 | -2.0 | ±1.9 | -3.0 | ±1.9 |
| -"- | mel | 2.0 | ±0.7 | -1.8 | ±1.9 | -2.9 | ±1.9 |
| -"- | mel | 1.9 | ±0.7 | -1.7 | ±1.9 | -2.7 | ±1.9 |
| -"- | mel | -12.6 | ±0.8 | -15.8 | ±1.9 | -9.3 | ±1.9 |
| -"- | mel | -9.7 | ±0.7 | -13.2 | ±1.8 | -8.1 | ±1.9 |
| -"- | mel | -5.9 | ±0.6 | -9.9 | ±1.9 | -6.8 | ±1.9 |
| -"- | mel | 2.5 | ±0.6 | -1.2 | ±1.9 | -2.5 | ±1.9 |
| -"- | mel | -32.3 | ±1.1 | -34.7 | ±1.0 | -17.9 | ±1.1 |

DOI: https://doi.org/10.2138/am-2024-9435. http://www.minsocam.org/

| | | | | | | | |
|---|---|---|---|---|---|---|---|
| -"- | mel | -26.6 | ±1.1 | -29.3 | ±1.0 | -15.4 | ±1.2 |
| -"- | mel | -11.5 | ±1.2 | -15.1 | ±1.1 | -9.1 | ±1.2 |
| -"- | mel | -3.1 | ±1.1 | -6.6 | ±1.0 | -5.0 | ±1.2 |
| -"- | mel | -1.7 | ±1.1 | -5.6 | ±1.0 | -4.7 | ±1.2 |
| -"- | mel | -1.8 | ±1.1 | -5.9 | ±1.0 | -4.9 | ±1.2 |
| -"- | mel | -2.0 | ±1.1 | -6.3 | ±1.0 | -5.2 | ±1.2 |
| -"- | mel | -2.3 | ±1.1 | -6.4 | ±1.0 | -5.2 | ±1.2 |
| -"- | mel | -8.5 | ±1.2 | -13.9 | ±1.0 | -9.5 | ±1.2 |
| -"- | mel | -2.9 | ±1.1 | -7.1 | ±1.0 | -5.6 | ±1.2 |
| -"- | mel | -2.1 | ±1.1 | -6.6 | ±1.0 | -5.5 | ±1.2 |
| -"- | mel | -2.0 | ±1.1 | -6.1 | ±1.1 | -5.1 | ±1.2 |
| -"- | mel | -1.1 | ±1.1 | -5.3 | ±1.1 | -4.7 | ±1.2 |
| -"- | mel | -0.7 | ±1.1 | -4.9 | ±1.0 | -4.6 | ±1.2 |
| -"- | mel | -10.0 | ±1.1 | -14.6 | ±1.0 | -9.4 | ±1.1 |
| -"- | mel | -17.3 | ±1.1 | -21.0 | ±1.0 | -12.1 | ±1.2 |
| -"- | mel | -30.5 | ±1.1 | -33.1 | ±1.1 | -17.2 | ±1.2 |
| -"- | mel | 3.0 | ±1.1 | -1.7 | ±1.0 | -3.3 | ±1.1 |
| -"- | mel | 3.7 | ±1.1 | -1.2 | ±1.1 | -3.1 | ±1.2 |
| -"- | mel | 3.0 | ±1.1 | -1.4 | ±1.0 | -3.0 | ±1.2 |
| -"- | mel | -31.5 | ±1.1 | -34.6 | ±1.1 | -18.2 | ±1.3 |
| -"- | mel | -2.0 | ±1.2 | -6.3 | ±1.0 | -5.2 | ±1.2 |
| -"- | mel | -2.6 | ±1.1 | -6.9 | ±1.0 | -5.5 | ±1.2 |
| -"- | pv | -23.3 | ±0.8 | -24.4 | ±1.5 | -12.3 | ± 1.5 |
| -"- | pv | -15.3 | ±0.8 | -11.7 | ±1.5 | -3.7 | ± 1.5 |
| -"- | pv | -15.2 | ±0.8 | -11.8 | ±1.5 | -3.9 | ± 1.5 |
| -"- | pv | -13.4 | ±0.8 | -10.8 | ±1.5 | -3.9 | ± 1.6 |
| -"- | pv | -33.0 | ±0.8 | -32.4 | ±1.5 | -15.2 | ± 1.6 |
| -"- | pv | -13.8 | ±0.8 | -10.4 | ±1.5 | -3.2 | ± 1.6 |
| -"- | rb | -37.2 | ±0.8 | -40.9 | ±1.5 | -21.6 | ± 1.6 |
| -"- | rb | -19.6 | ±0.8 | -22.6 | ±1.6 | -12.4 | ± 1.6 |
| -"- | rb | -33.1 | ±0.8 | -32.9 | ±1.6 | -15.7 | ± 1.6 |
| -"- | rb | -16.7 | ±0.8 | -17.6 | ±1.5 | -8.9 | ± 1.6 |
| -"- | rb | -5.4 | ±0.8 | -9.6 | ±1.6 | -6.7 | ± 1.7 |
| -"- | rb | -31.5 | ±0.8 | -34.9 | ±1.6 | -18.5 | ± 1.6 |
| -"- | rb | -17.1 | ±0.8 | -20.9 | ±1.6 | -11.9 | ± 1.6 |
| -"- | rb | -5.7 | ±0.8 | -11.4 | ±1.6 | -8.4 | ± 1.7 |
| -"- | sp | -49.0 | ±0.9 | -48.7 | ±1.8 | -23.2 | ± 1.8 |
| -"- | sp | -48.2 | ±0.9 | -50.9 | ±1.8 | -25.9 | ± 1.8 |
| *E101* | | | | | | | |
| -"- | mel | -7.1 | ±0.8 | -12.8 | ±1.0 | -9.1 | ± 1.1 |
| -"- | mel | -3.6 | ±0.8 | -10.2 | ±1.0 | -8.4 | ± 1.1 |

| | | | | | | | |
|---|---|---|---|---|---|---|---|
| -"- | mel | -2.4 | ±0.8 | -9.4 | ±1.0 | -8.2 | ± 1.1 |
| -"- | mel | -4.4 | ±0.9 | -10.4 | ±1.0 | -8.1 | ± 1.1 |
| -"- | mel | -2.5 | ±0.9 | -9.1 | ±1.1 | -7.8 | ± 1.1 |
| -"- | mel | -3.9 | ±0.8 | -9.6 | ±1.0 | -7.6 | ± 1.1 |
| -"- | mel | -3.8 | ±0.8 | -9.5 | ±1.0 | -7.5 | ± 1.1 |
| -"- | mel | -4.3 | ±0.9 | -9.7 | ±1.1 | -7.5 | ± 1.2 |
| -"- | mel | -2.9 | ±0.8 | -8.9 | ±1.0 | -7.4 | ± 1.1 |
| -"- | mel | -5.2 | ±1.0 | -9.9 | ±1.1 | -7.2 | ± 1.2 |
| -"- | mel | -0.9 | ±0.8 | -7.5 | ±1.0 | -7.1 | ± 1.1 |
| -"- | mel | -3.2 | ±0.9 | -8.7 | ±1.0 | -7.0 | ± 1.1 |
| -"- | mel | -2.5 | ±0.8 | -8.3 | ±1.0 | -7.0 | ± 1.1 |
| -"- | mel | -0.7 | ±0.8 | -7.0 | ±1.0 | -6.6 | ± 1.1 |
| -"- | mel | 3.1 | ±1.0 | -3.6 | ±1.0 | -5.2 | ± 1.1 |
| -"- | mel | 6.3 | ±0.8 | -0.9 | ±1.0 | -4.2 | ± 1.1 |
| -"- | mel | 6.0 | ±0.8 | -1.0 | ±1.0 | -4.1 | ± 1.1 |
| -"- | mel | 6.2 | ±0.8 | -0.8 | ±1.0 | -4.1 | ± 1.1 |
| -"- | mel | 6.8 | ±0.8 | -0.4 | ±1.0 | -4.0 | ± 1.1 |
| -"- | mel | 5.9 | ±0.8 | -0.7 | ±1.0 | -3.8 | ± 1.1 |
| -"- | mel | 7.2 | ±0.8 | 0.2 | ±1.0 | -3.6 | ± 1.1 |
| -"- | mel | 7.1 | ±0.8 | 0.1 | ±1.0 | -3.5 | ± 1.1 |
| -"- | mel | 6.6 | ±0.8 | 0.1 | ±1.0 | -3.4 | ± 1.1 |
| -"- | mel | 6.1 | ±0.8 | -0.2 | ±1.0 | -3.4 | ± 1.1 |
| -"- | pv | -57.5 | ±1.0 | -53.3 | ±1.7 | -23.4 | ± 1.7 |
| -"- | pv | -59.4 | ±1.0 | -54.3 | ±1.7 | -23.4 | ± 1.7 |
| -"- | pv | -58.8 | ±1.0 | -53.8 | ±1.7 | -23.3 | ± 1.7 |
| -"- | pv | -59.7 | ±1.0 | -53.5 | ±1.7 | -22.5 | ± 1.7 |
| -"- | pv | -61.1 | ±1.0 | -54.2 | ±1.6 | -22.4 | ± 1.7 |
| -"- | pv | -58.4 | ±1.0 | -52.5 | ±1.7 | -22.1 | ± 1.7 |
| -"- | pv | -40.4 | ±1.0 | -36.7 | ±1.7 | -15.7 | ± 1.7 |
| -"- | rb | -51.8 | ±1.0 | -48.5 | ±1.7 | -21.6 | ± 1.8 |
| -"- | rb | -45.2 | ±1.0 | -43.0 | ±1.7 | -19.6 | ± 1.8 |
| -"- | rb | -42.3 | ±1.0 | -40.8 | ±1.7 | -18.7 | ± 1.8 |
| -"- | rb | -41.6 | ±1.0 | -38.8 | ±1.7 | -17.2 | ± 1.8 |
| -"- | rb | -18.8 | ±1.0 | -20.1 | ±1.7 | -10.3 | ± 1.8 |
| -"- | sp | -52.1 | ±1.1 | -50.3 | ±1.9 | -23.2 | ± 2.0 |
| -"- | sp | -53.3 | ±1.1 | -51.1 | ±1.9 | -23.4 | ± 2.0 |
| *E105* | mel | -7.9 | ±1.5 | -13.7 | ±0.6 | -9.6 | ± 1.0 |
| -"- | mel | -8.2 | ±1.5 | -13.6 | ±0.7 | -9.3 | ± 1.0 |
| -"- | mel | -8.0 | ±1.5 | -13.5 | ±0.6 | -9.3 | ± 1.0 |
| -"- | mel | -7.9 | ±1.5 | -13.4 | ±0.6 | -9.3 | ± 1.0 |
| -"- | mel | -8.1 | ±1.5 | -13.3 | ±0.7 | -9.1 | ± 1.0 |

| | | | | | | | |
|---|---|---|---|---|---|---|---|
| -"- | mel | -8.6 | ±1.5 | -13.2 | ±0.7 | -8.7 | ± 1.0 |
| -"- | mel | -1.8 | ±1.5 | -8.6 | ±0.6 | -7.7 | ± 1.0 |
| -"- | mel | -0.9 | ±1.5 | -7.8 | ±0.7 | -7.3 | ± 1.0 |
| -"- | mel | -0.4 | ±1.5 | -7.1 | ±0.6 | -6.9 | ± 1.0 |
| -"- | mel | 0.0 | ±1.5 | -6.9 | ±0.7 | -6.9 | ± 1.0 |
| -"- | mel | -1.4 | ±1.5 | -7.6 | ±0.7 | -6.9 | ± 1.0 |
| -"- | mel | -1.3 | ±1.5 | -7.4 | ±0.6 | -6.7 | ± 1.0 |
| -"- | mel | -0.1 | ±1.5 | -6.5 | ±0.6 | -6.5 | ± 1.0 |
| -"- | mel | 1.4 | ±1.5 | -5.6 | ±0.6 | -6.4 | ± 1.0 |
| -"- | mel | 2.7 | ±1.5 | -4.3 | ±0.6 | -5.7 | ± 1.0 |
| -"- | mel | 2.9 | ±1.5 | -4.2 | ±0.7 | -5.7 | ± 1.0 |
| -"- | pv | -52.4 | ±1.6 | -51.1 | ±1.7 | -23.9 | ± 1.9 |
| -"- | pv | -51.7 | ±1.6 | -50.2 | ±1.7 | -23.3 | ± 1.9 |
| -"- | pv | -53.4 | ±1.6 | -50.4 | ±1.7 | -22.6 | ± 1.9 |
| -"- | pv | -47.2 | ±1.6 | -46.1 | ±1.7 | -21.6 | ± 1.9 |
| -"- | pv | -47.9 | ±1.6 | -45.2 | ±1.8 | -20.3 | ± 1.9 |
| -"- | pv | -40.6 | ±1.6 | -39.6 | ±1.8 | -18.5 | ± 1.9 |
| -"- | pv | -37.9 | ±1.6 | -37.8 | ±1.7 | -18.1 | ± 1.9 |
| -"- | rb | -41.6 | ±1.6 | -44.2 | ±1.8 | -22.6 | ± 2.0 |
| -"- | rb | -40.8 | ±1.6 | -43.8 | ±1.8 | -22.6 | ± 2.0 |
| -"- | rb | -43.4 | ±1.6 | -44.8 | ±1.8 | -22.3 | ± 2.0 |
| -"- | rb | -41.7 | ±1.6 | -43.4 | ±1.8 | -21.7 | ± 2.0 |
| -"- | rb | -38.4 | ±1.6 | -41.1 | ±1.8 | -21.2 | ± 2.0 |
| -"- | rb | -33.7 | ±1.6 | -37.2 | ±1.8 | -19.6 | ± 2.0 |
| -"- | rb | -35.7 | ±1.6 | -36.0 | ±1.8 | -17.4 | ± 2.0 |
| -"- | rb | -28.1 | ±1.6 | -30.6 | ±1.8 | -15.9 | ± 2.0 |
| -"- | rb | -32.1 | ±1.6 | -32.6 | ±1.8 | -15.9 | ± 2.0 |
| -"- | sp | -45.5 | ±1.6 | -46.7 | ±2.0 | -23.0 | ± 2.2 |
| -"- | sp | -45.2 | ±1.6 | -48.4 | ±2.1 | -24.8 | ± 2.2 |
| -"- | sp | -47.4 | ±1.6 | -48.2 | ±2.0 | -23.5 | ± 2.2 |
| -"- | sp | -47.4 | ±1.6 | -48.5 | ±2.0 | -23.9 | ± 2.1 |
| *40E* | cpx | 6.5 | ±1.1 | -1.6 | ±1.5 | -4.9 | ± 1.6 |
| -"- | cpx | 6.5 | ±1.1 | -2.4 | ±1.5 | -5.8 | ± 1.6 |
| -"- | cpx | 6.5 | ±1.1 | -1.1 | ±1.5 | -4.5 | ± 1.6 |
| -"- | cpx | 8.0 | ±1.1 | -1.3 | ±1.6 | -5.5 | ± 1.7 |
| -"- | cpx | 8.6 | ±1.1 | -0.9 | ±1.5 | -5.3 | ± 1.7 |
| -"- | cpx | 7.2 | ±1.1 | 1.0 | ±1.5 | -2.8 | ± 1.7 |
| -"- | cpx | -3.8 | ±1.1 | -7.2 | ±1.5 | -5.2 | ± 1.6 |
| -"- | cpx | -6.0 | ±1.1 | -8.8 | ±1.5 | -5.6 | ± 1.6 |
| -"- | cpx | -19.6 | ±1.1 | -21.1 | ±1.5 | -10.9 | ± 1.6 |
| -"- | cpx | -1.7 | ±1.1 | -6.5 | ±1.5 | -5.6 | ± 1.6 |

| | | | | | | | |
|---|---|---|---|---|---|---|---|
| -"- | cpx | 1.8 | ±1.1 | -3.1 | ±1.5 | -4.0 | ± 1.6 |
| -"- | cpx | -37.0 | ±1.1 | -40.4 | ±1.6 | -21.1 | ± 1.7 |
| -"- | cpx | -24.7 | ±1.2 | -29.5 | ±1.7 | -16.7 | ± 1.8 |
| -"- | mel | 2.5 | ±1.1 | -5.6 | ±1.6 | -6.9 | ± 1.7 |
| -"- | mel | 0.4 | ±1.1 | -6.6 | ±1.6 | -6.8 | ± 1.7 |
| -"- | mel | 1.7 | ±1.2 | -4.9 | ±1.6 | -5.8 | ± 1.7 |
| -"- | mel | 1.3 | ±1.2 | -4.4 | ±1.6 | -5.1 | ± 1.7 |
| -"- | mel | 1.5 | ±1.2 | -4.9 | ±1.6 | -5.6 | ± 1.7 |
| -"- | mel | 0.8 | ±1.2 | -4.8 | ±1.6 | -5.2 | ± 1.7 |
| -"- | mel | -23.9 | ±1.2 | -27.4 | ±1.7 | -15.0 | ± 1.8 |
| -"- | mel | -16.0 | ±1.2 | -20.4 | ±1.7 | -12.0 | ± 1.9 |
| -"- | mel | -33.6 | ±1.2 | -37.4 | ±1.7 | -20.0 | ± 1.8 |
| -"- | mel | -8.1 | ±1.1 | -11.2 | ±1.5 | -7.0 | ± 1.6 |
| -"- | mel | -31.8 | ±1.2 | -34.2 | ±1.6 | -17.7 | ± 1.7 |
| -"- | mel | -38.7 | ±1.2 | -42.4 | ±1.7 | -22.3 | ± 1.8 |
| -"- | pv | -35.9 | ±1.8 | -35.8 | ±1.7 | -17.2 | ± 1.9 |
| -"- | pv | -48.2 | ±1.7 | -46.8 | ±1.7 | -21.8 | ± 1.9 |
| -"- | pv | -51.7 | ±1.7 | -50.4 | ±1.5 | -23.5 | ± 1.7 |
| -"- | pv | -52.3 | ±1.7 | -51.0 | ±1.5 | -23.8 | ± 1.7 |
| -"- | pv | -50.8 | ±1.7 | -50.5 | ±1.7 | -24.1 | ± 1.9 |
| -"- | pv | -47.3 | ±1.7 | -48.1 | ±1.7 | -23.5 | ± 1.9 |
| -"- | pv | -28.4 | ±1.7 | -31.4 | ±1.5 | -16.7 | ± 1.7 |
| -"- | pv | -48.7 | ±1.7 | -49.2 | ±1.5 | -23.9 | ± 1.7 |
| -"- | pv | -21.0 | ±1.8 | -23.0 | ±1.8 | -12.0 | ± 2.0 |
| -"- | pv | -46.0 | ±1.8 | -45.8 | ±1.8 | -21.9 | ± 2.0 |
| -"- | rb | -43.9 | ±1.1 | -45.6 | ±1.4 | -22.8 | ± 1.5 |
| -"- | rb | -40.9 | ±1.1 | -42.5 | ±1.4 | -21.2 | ± 1.5 |
| -"- | rb | -39.1 | ±1.1 | -38.7 | ±1.4 | -18.4 | ± 1.5 |
| -"- | rb | -39.4 | ±1.1 | -41.1 | ±1.4 | -20.6 | ± 1.5 |
| -"- | sp | -46.9 | ±1.7 | -48.2 | ±1.7 | -23.8 | ± 1.9 |
| -"- | sp | -48.4 | ±1.7 | -48.6 | ±1.5 | -23.5 | ± 1.7 |
| -"- | sp | -45.9 | ±1.7 | -47.9 | ±1.5 | -24.0 | ± 1.7 |
| -"- | sp | -41.7 | ±1.7 | -46.4 | ±1.5 | -24.7 | ± 1.8 |
| -"- | sp | -43.7 | ±1.7 | -47.8 | ±1.5 | -25.0 | ± 1.7 |
| *V3* | cpx | -47.1 | ±3.4 | -50.7 | ±4.8 | -26.2 | ±5.2 |
| -"- | dav | 6.9 | ±3.3 | -3.5 | ±6.9 | -7.1 | ±7.1 |
| -"- | dav | -0.1 | ±3.2 | -9.0 | ±6.5 | -9.0 | ±6.7 |
| -"- | dav | 6.1 | ±3.0 | -6.2 | ±5.8 | -9.4 | ±6.0 |
| -"- | dav | 2.8 | ±3.5 | -0.8 | ±5.7 | -2.2 | ±6.0 |
| -"- | dav | 9.8 | ±3.0 | 3.9 | ±7.0 | -1.2 | ±7.2 |
| -"- | dav | 8.9 | ±3.3 | 0.4 | ±5.2 | -4.2 | ±5.4 |

DOI: https://doi.org/10.2138/am-2024-9435. http://www.minsocam.org/

| | | | | | | | |
|---|---|---|---|---|---|---|---|
| -"- | ern | -10.0 | ±3.2 | -12.7 | ±5.7 | -7.4 | ±6.0 |
| -"- | ern | -2.0 | ±3.2 | -8.5 | ±5.8 | -7.5 | ±6.1 |
| -"- | fo | -48.5 | ±3.1 | -51.8 | ±5.7 | -26.5 | ±5.9 |
| -"- | fo | -43.0 | ±3.4 | -45.3 | ±4.6 | -22.9 | ±4.9 |
| -"- | fo | -44.6 | ±3.9 | -44.7 | ±5.7 | -21.5 | ±6.1 |
| -"- | fo | -46.7 | ±3.7 | -48.6 | ±6.7 | -24.3 | ±6.9 |
| -"- | sp | -42.3 | ±2.9 | -46.9 | ±5.7 | -24.9 | ±5.9 |
| -"- | sp | -39.6 | ±3.1 | -48.5 | ±6.0 | -27.9 | ±6.2 |
| -"- | sp | -40.1 | ±3.0 | -43.6 | ±6.2 | -22.8 | ±6.4 |
| -"- | tzr | 4.8 | ±4.8 | -4.2 | ±4.7 | -6.7 | ±4.9 |

cpx = AlTi-diopside; ern = eringoite; dav = davisite; fo = forsterite;
grs = grossmanite; mel = melilite; pv = perovskite; rb = rubinite; sp = spinel;
tzr = tazheranite.

DOI: https://doi.org/10.2138/am-2024-9435. http://www.minsocam.org/

**Figure 1.** Vigarano UR *V3*

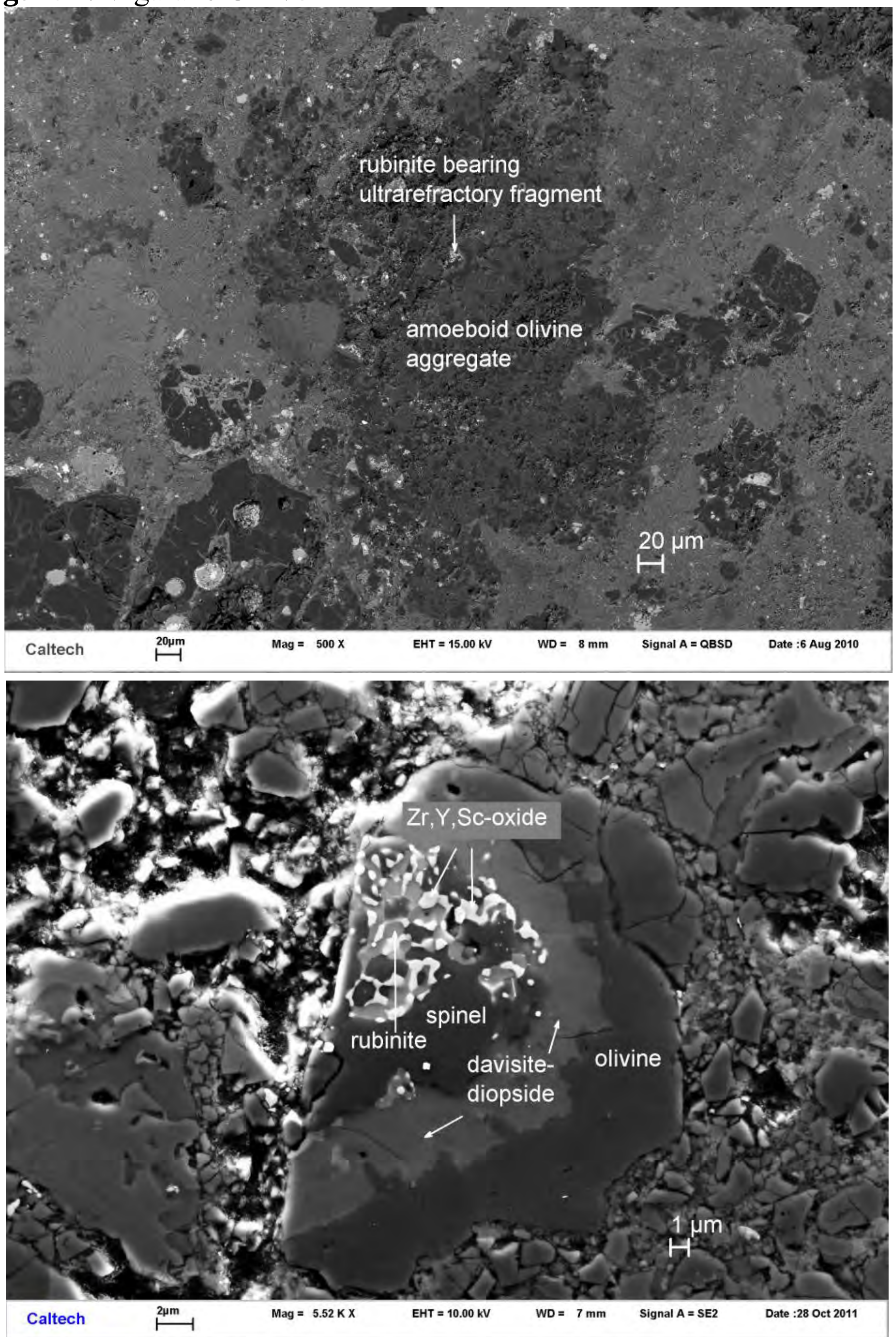


a.

b.

This is the peer-reviewed, final accepted version for American Mineralogist, published by the Mineralogical Society of America.
The published version is subject to change. Cite as Authors (Year) Title. American Mineralogist, in press.
DOI: https://doi.org/10.2138/am-2024-9435. http://www.minsocam.org/

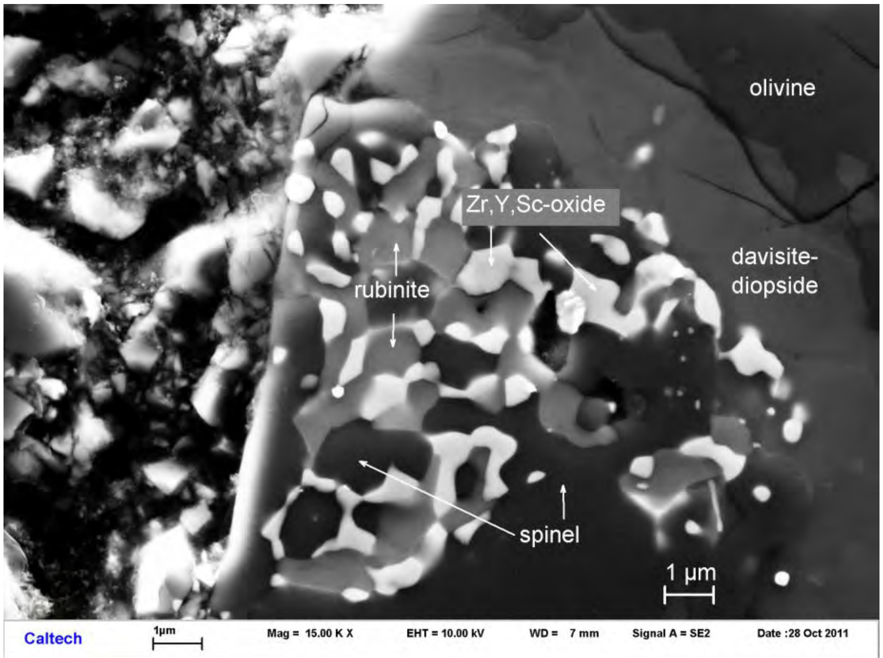


c.

**Figure 1**. Backscatter electron (BSE) images showing the ultrarefractory inclusion *V3* from Vigarano. Rubinite with Zr-Sc oxide and spinel is surrounded by a davisite-diopside intergrowth, with a rim of forsterite. Note the absence of perovskite in this inclusion.

**Figure 2.** Allende FTA *AE01-01*

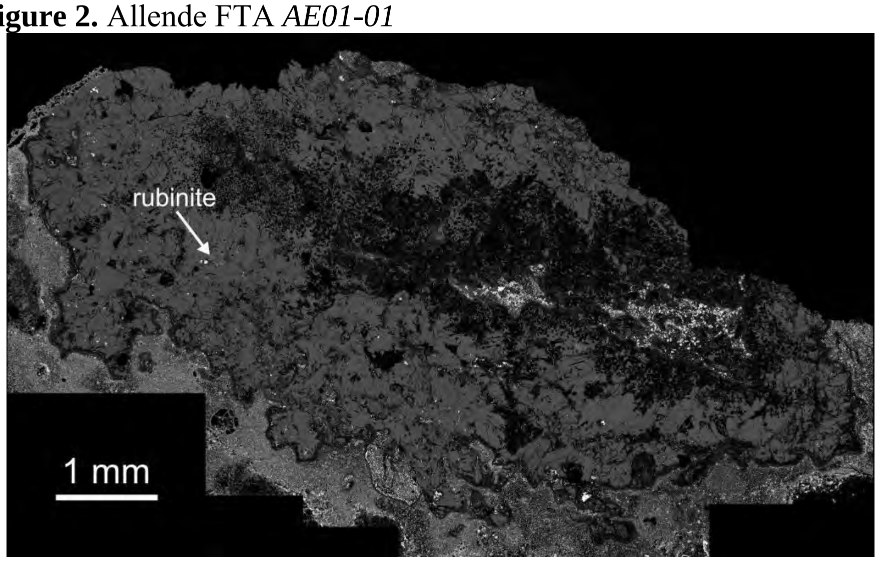


a.

b. 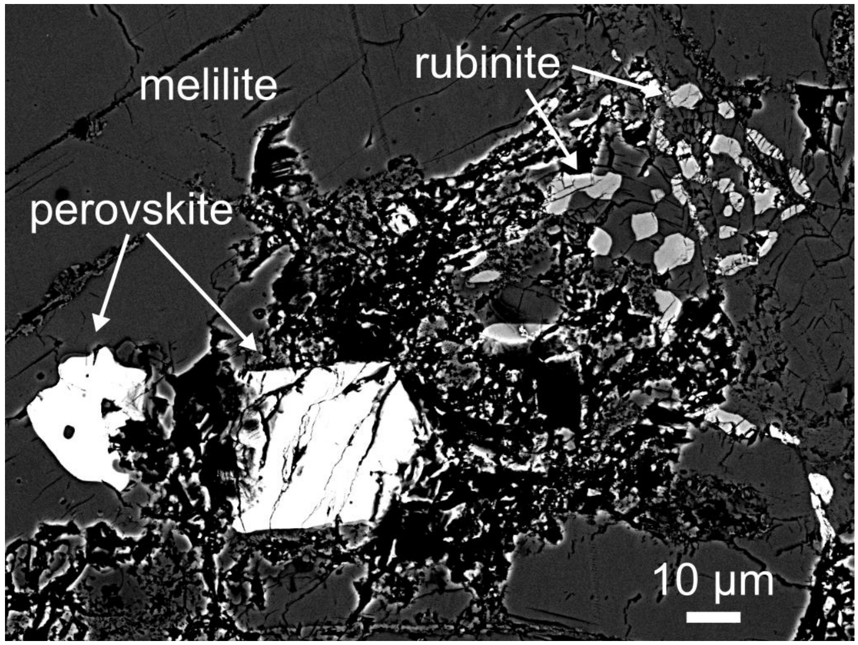


c. 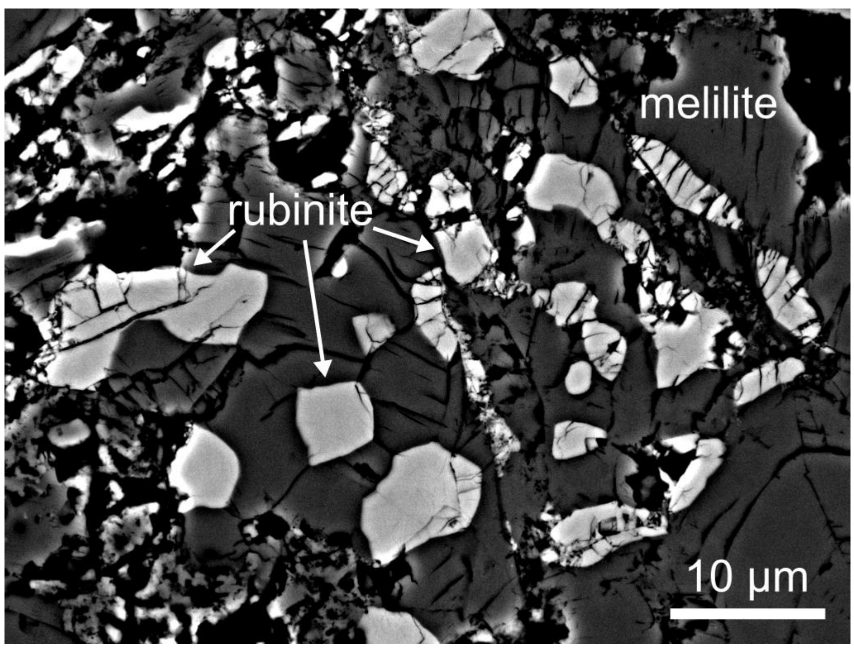


**Figure 2**. BSE images showing rubinite in FTA CAI *AE01-01* in Allende.

This is the peer-reviewed, final accepted version for American Mineralogist, published by the Mineralogical Society of America.
The published version is subject to change. Cite as Authors (Year) Title. American Mineralogist, in press.
DOI: https://doi.org/10.2138/am-2024-9435. http://www.minsocam.org/

**Figure 3.** Efremovka

a – CTA *E101*

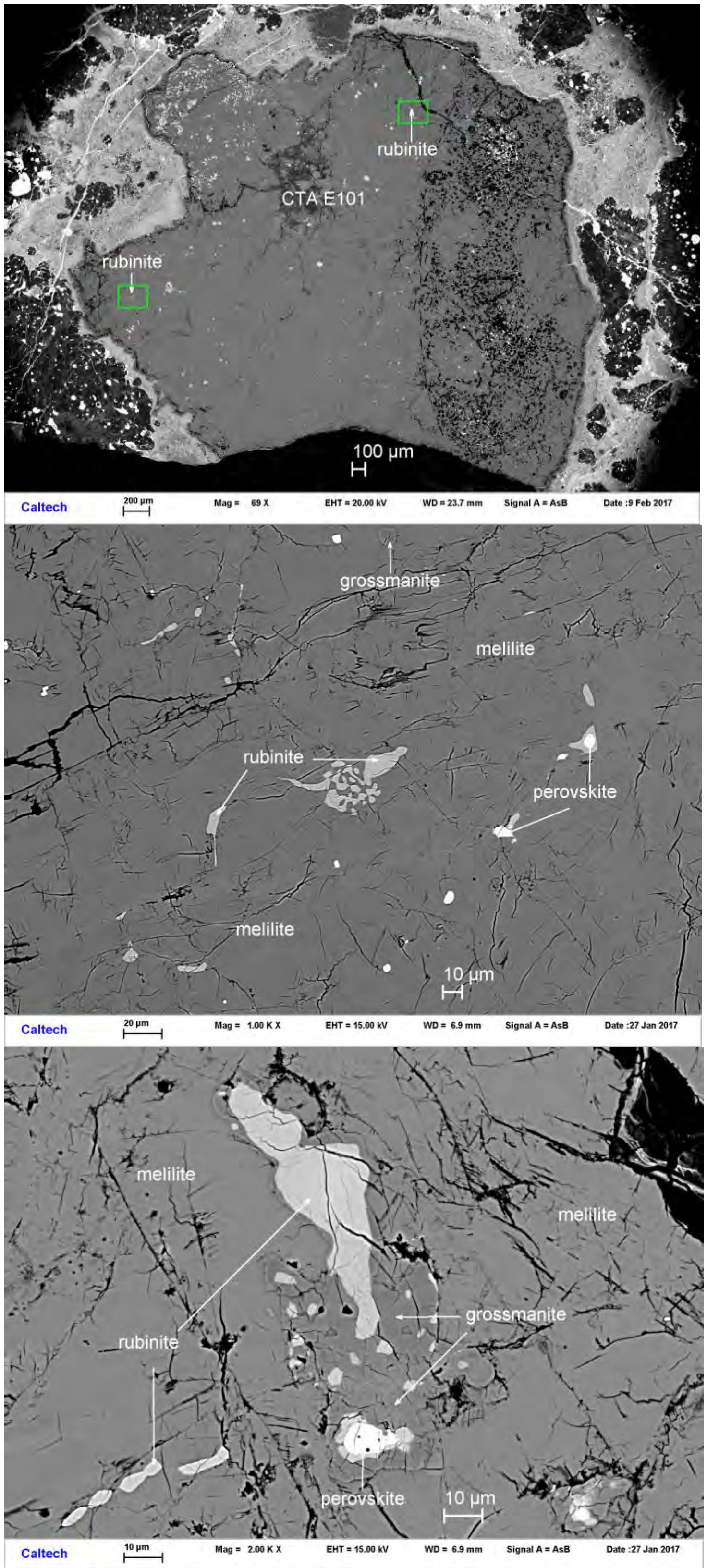

b – CTA *E105*

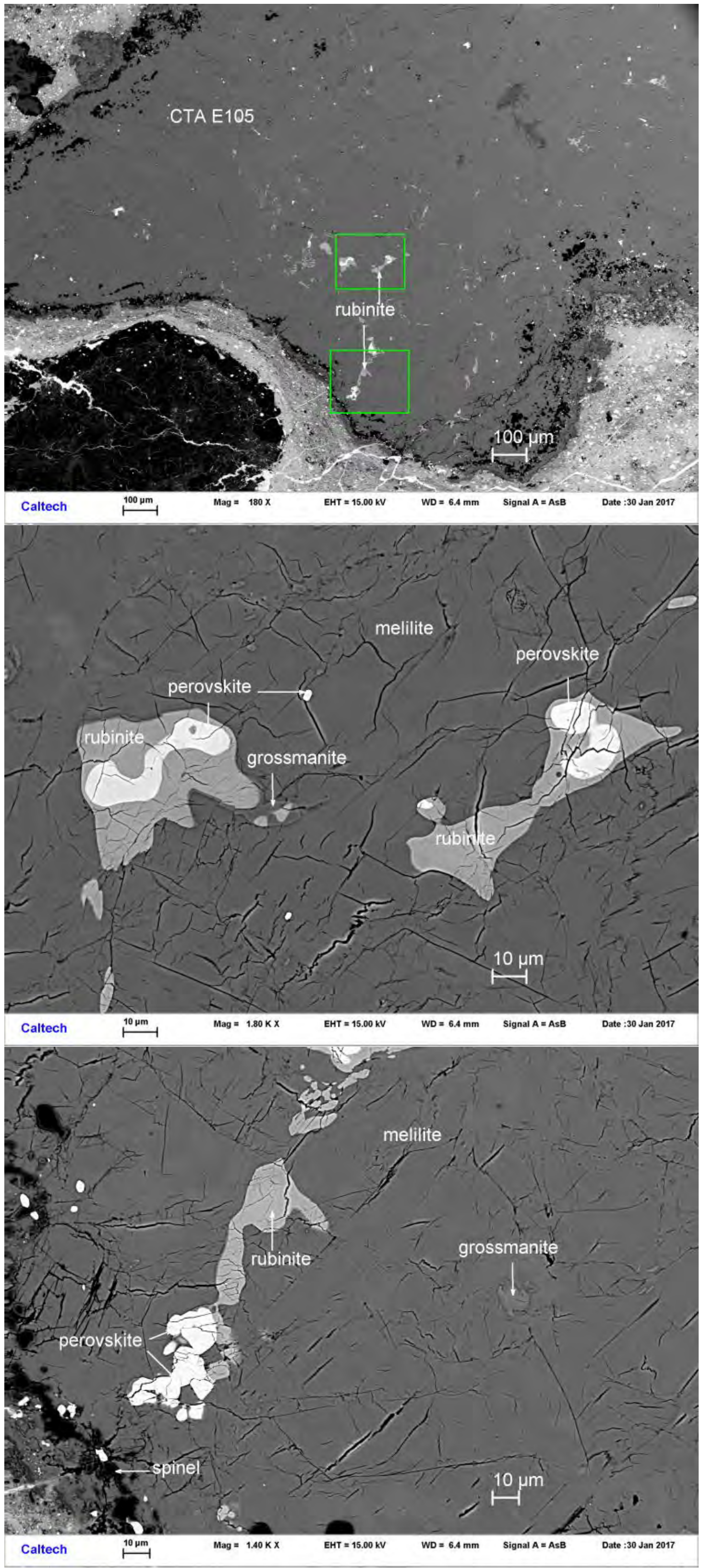
CTA E105
rubinite
100 µm
Caltech
Mag = 180 X
EHT = 15.00 kV
WD = 6.4 mm
Signal A = AsB
Date :30 Jan 2017
melilite
perovskite
perovskite
rubinite
grossmanite
rubinite
10 µm
Caltech
Mag = 1.80 K X
EHT = 15.00 kV
WD = 6.4 mm
Signal A = AsB
Date :30 Jan 2017
melilite
rubinite
grossmanite
perovskite
spinel
10 µm
Caltech
Mag = 1.40 K X
EHT = 15.00 kV
WD = 6.4 mm
Signal A = AsB
Date :30 Jan 2017

DOI: https://doi.org/10.2138/am-2024-9435. http://www.minsocam.org/

c – CTA *40E* & UR *40E-1*

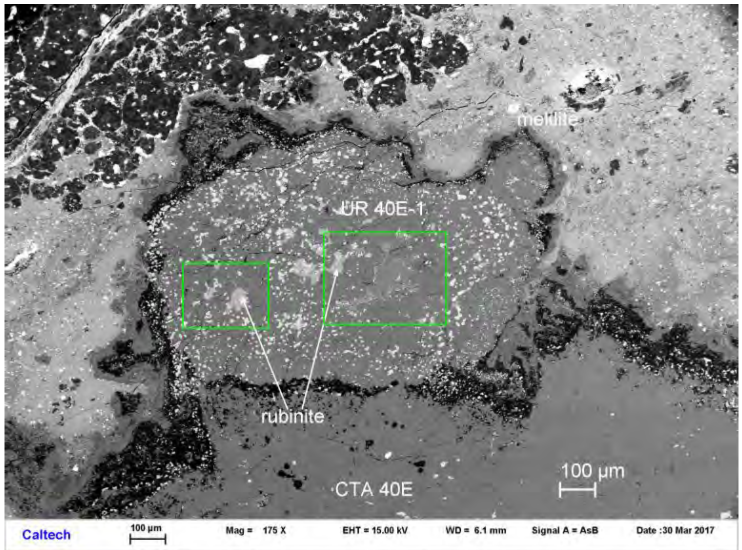


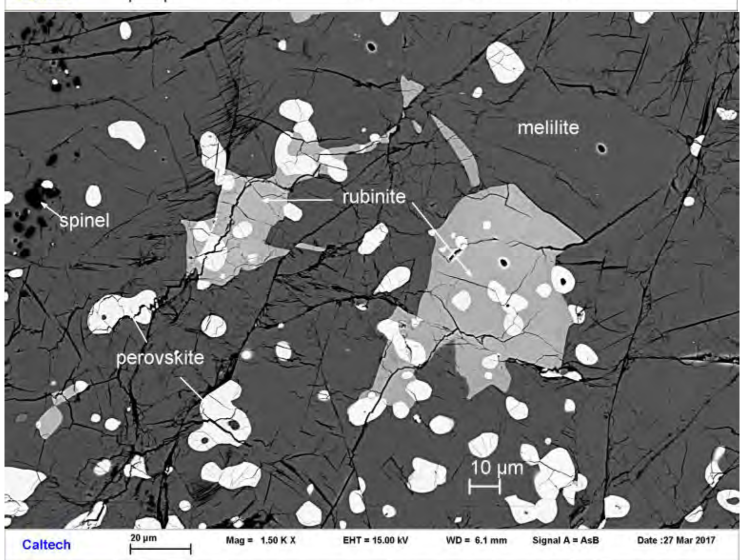


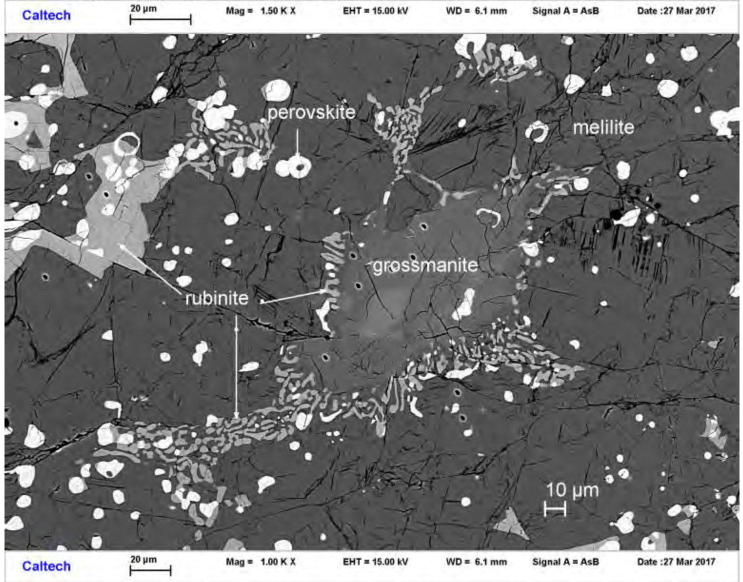

**Figure 3**. BSE images showing rubinite in three CAI inclusions in Efremovka. (a) CTA *E101*. (b) CTA *E105*. (c) CTA *E40E-1* and *UR40E-1*.

a – Vigarano *V3*

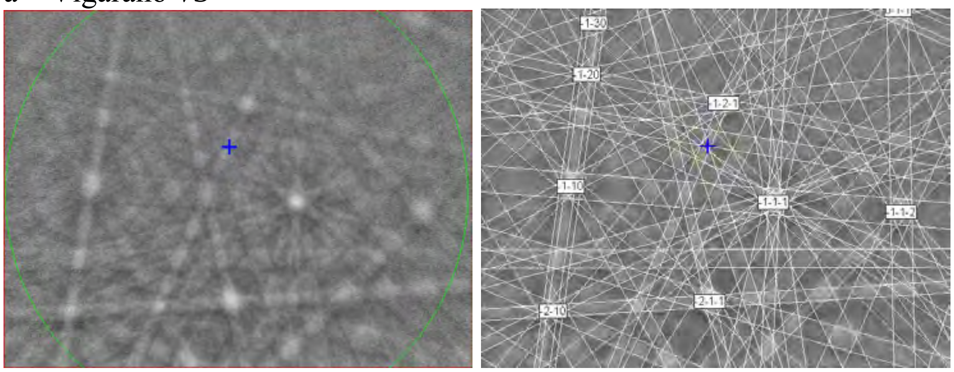

b – Allende *AE01-01*

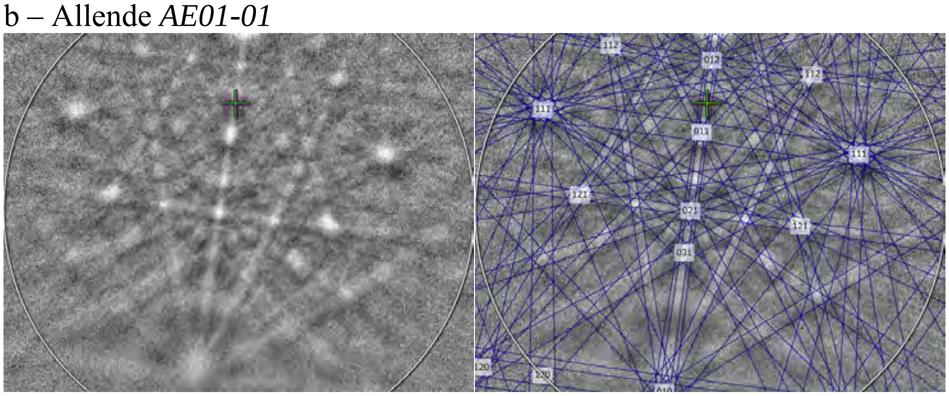

c – Efremovka *E105*

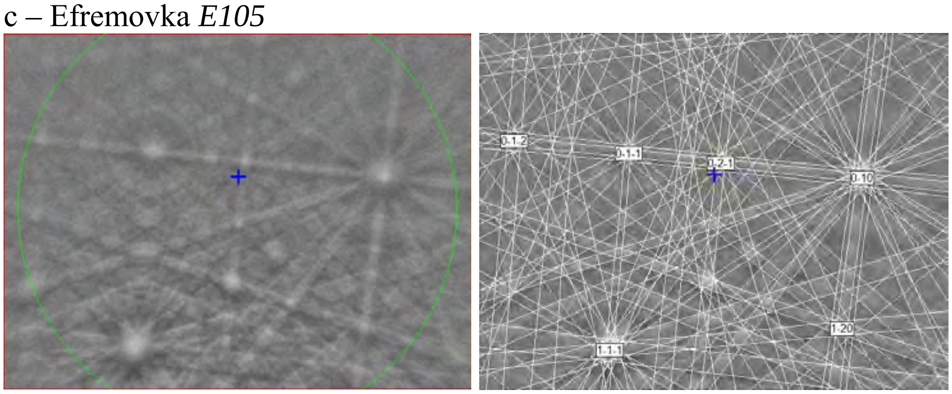

**Figure 4**. EBSD patterns of three rubinite crystals from (a) Vigarano *V3*, (b) Allende *AE01-01*, and (c) Efremovka *E105*. For each, the observed pattern is shown in the left panel, where a cross indicates the center of the EBSD pattern. The right panel shows the pattern indexed with the garnet structure.

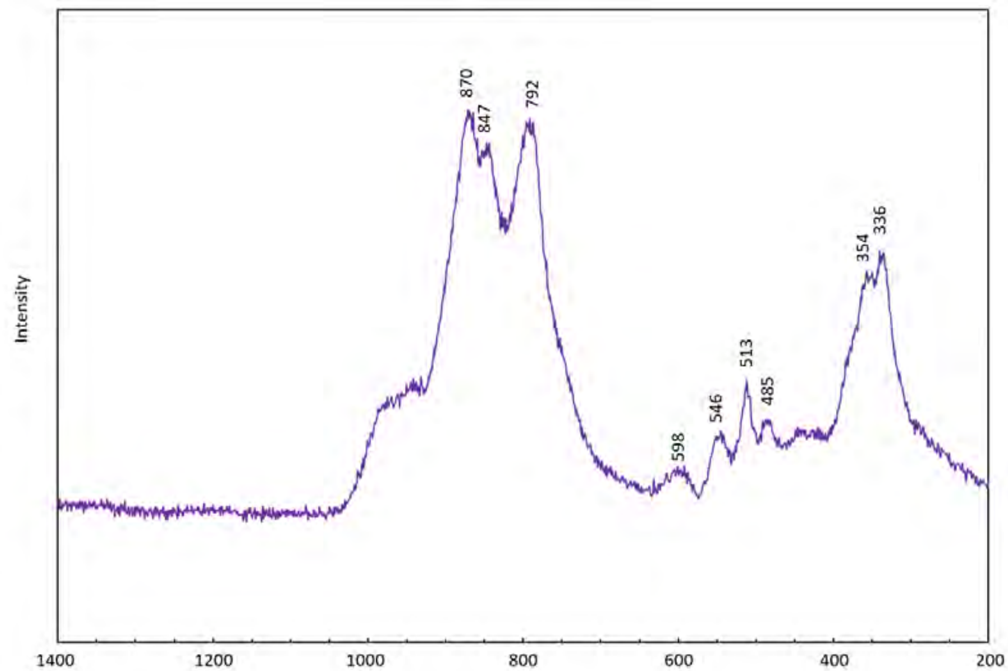


**Figure 5**. Raman spectra of rubinite from Efremovka inclusion *E101b* using a green laser.

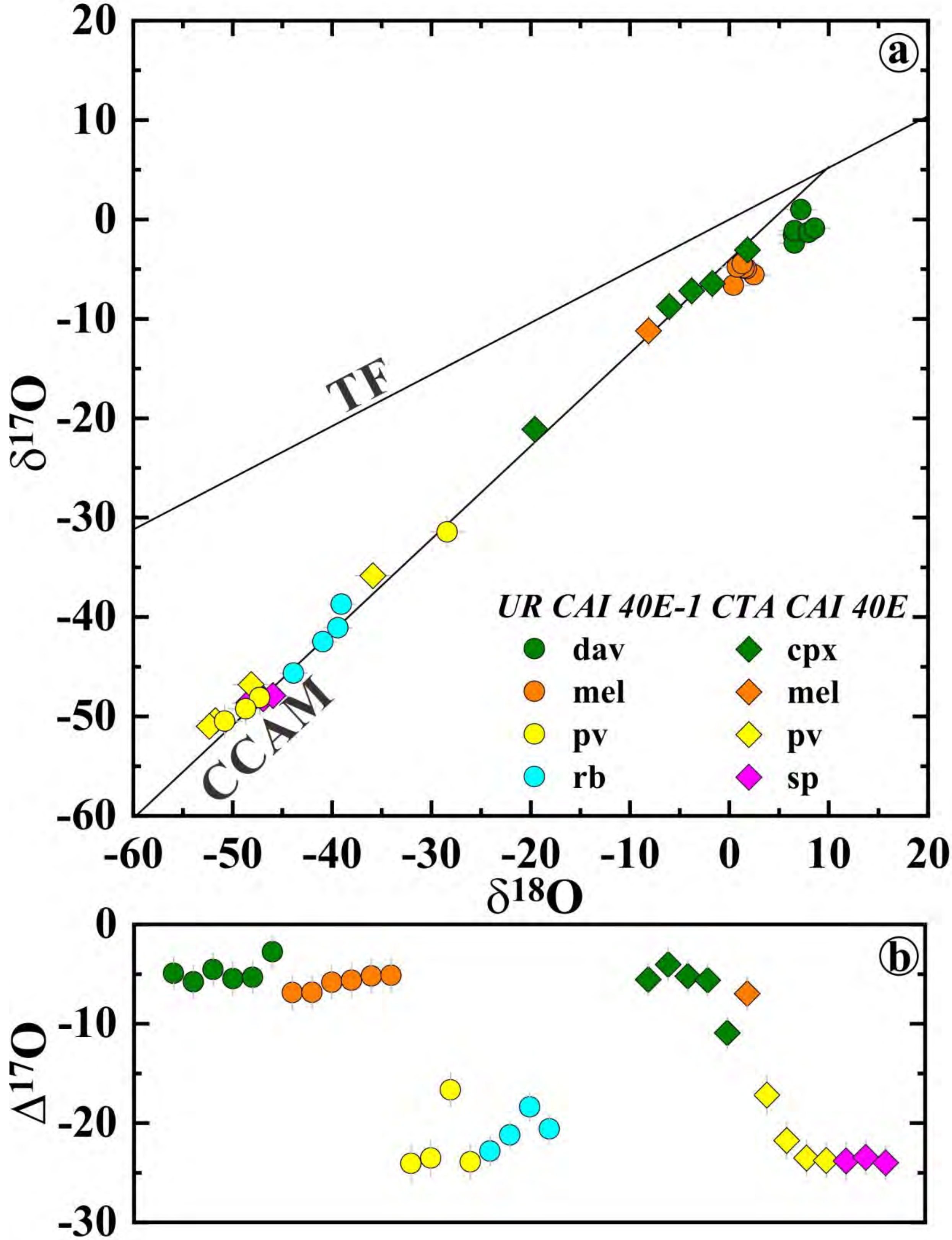
a
TF
CCAM
UR CAI 40E-1
CTA CAI 40E
dav
mel
pv
rb
cpx
mel
pv
sp
δ17O
δ18O
20
10
0
-10
-20
-30
-40
-50
-60
-60
-50
-40
-30
-20
-10
0
10
20
b
Δ17O
0
-10
-20
-30

526

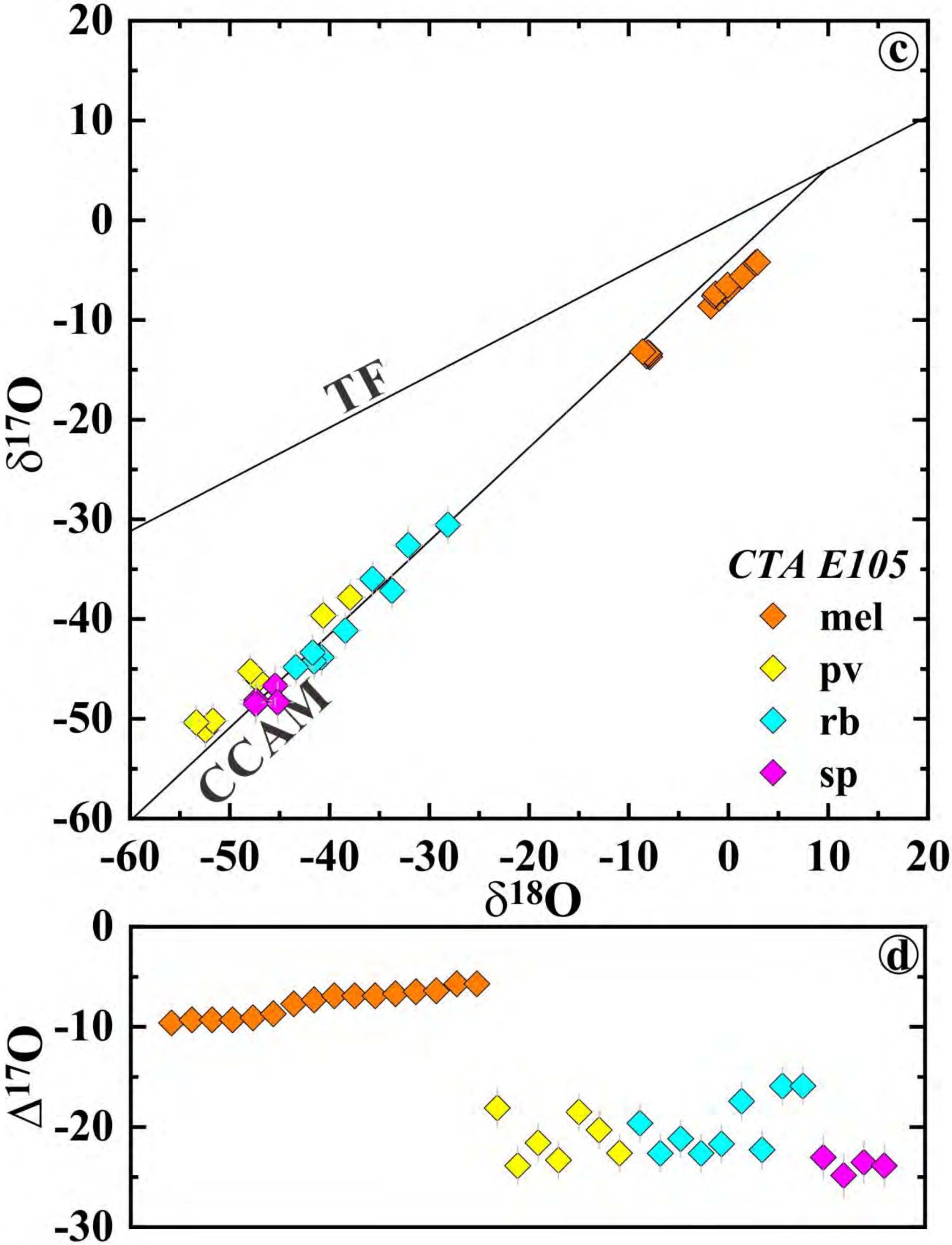
c
TF
CCAM
CTA E105
mel
pv
rb
sp
δ17O
δ18O
20
10
0
-10
-20
-30
-40
-50
-60
-60
-50
-40
-30
-20
-10
0
10
20
d
Δ17O
0
-10
-20
-30

527

This is the peer-reviewed, final accepted version for American Mineralogist, published by the Mineralogical Society of America.
The published version is subject to change. Cite as Authors (Year) Title. American Mineralogist, in press.
DOI: https://doi.org/10.2138/am-2024-9435. http://www.minsocam.org/

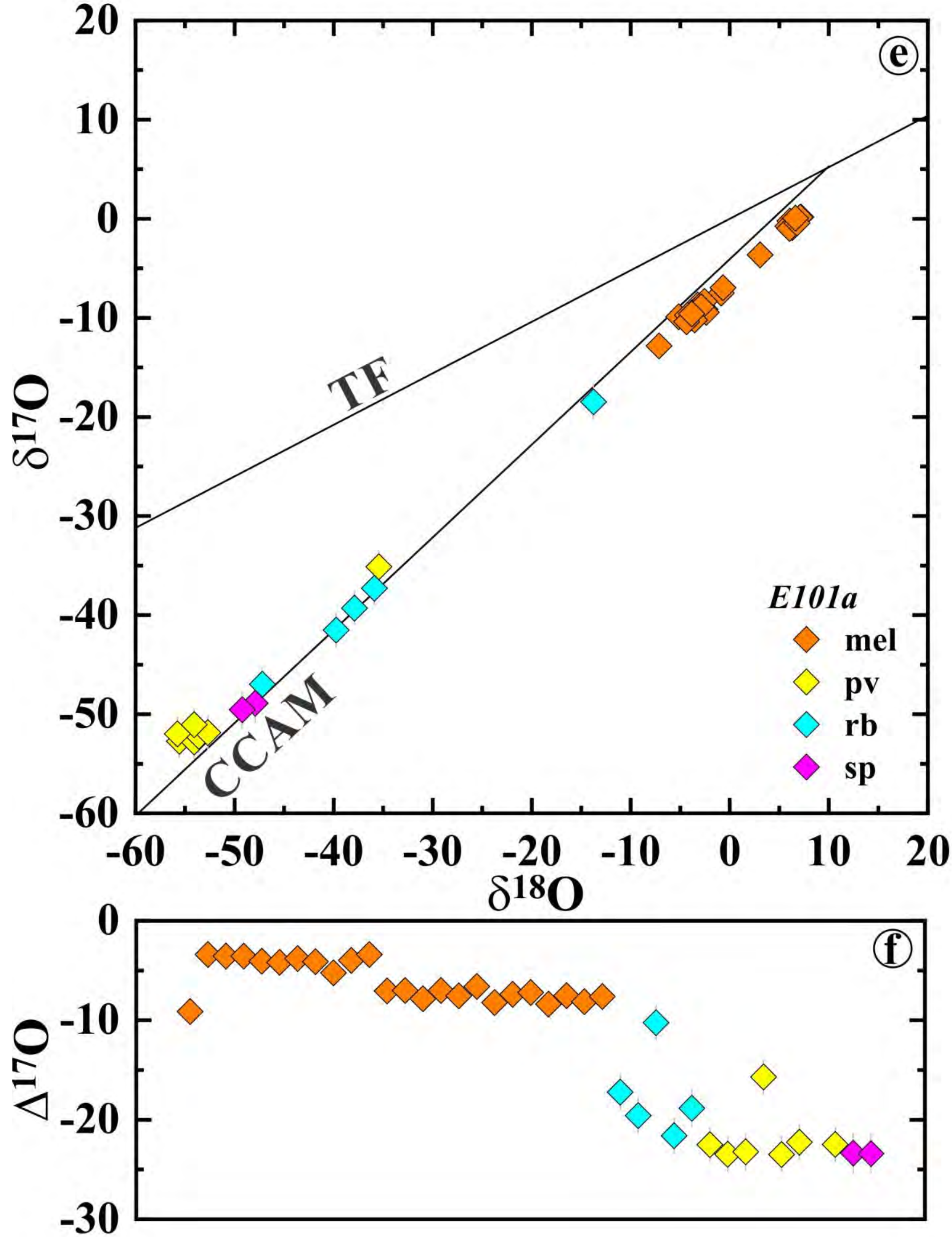


528

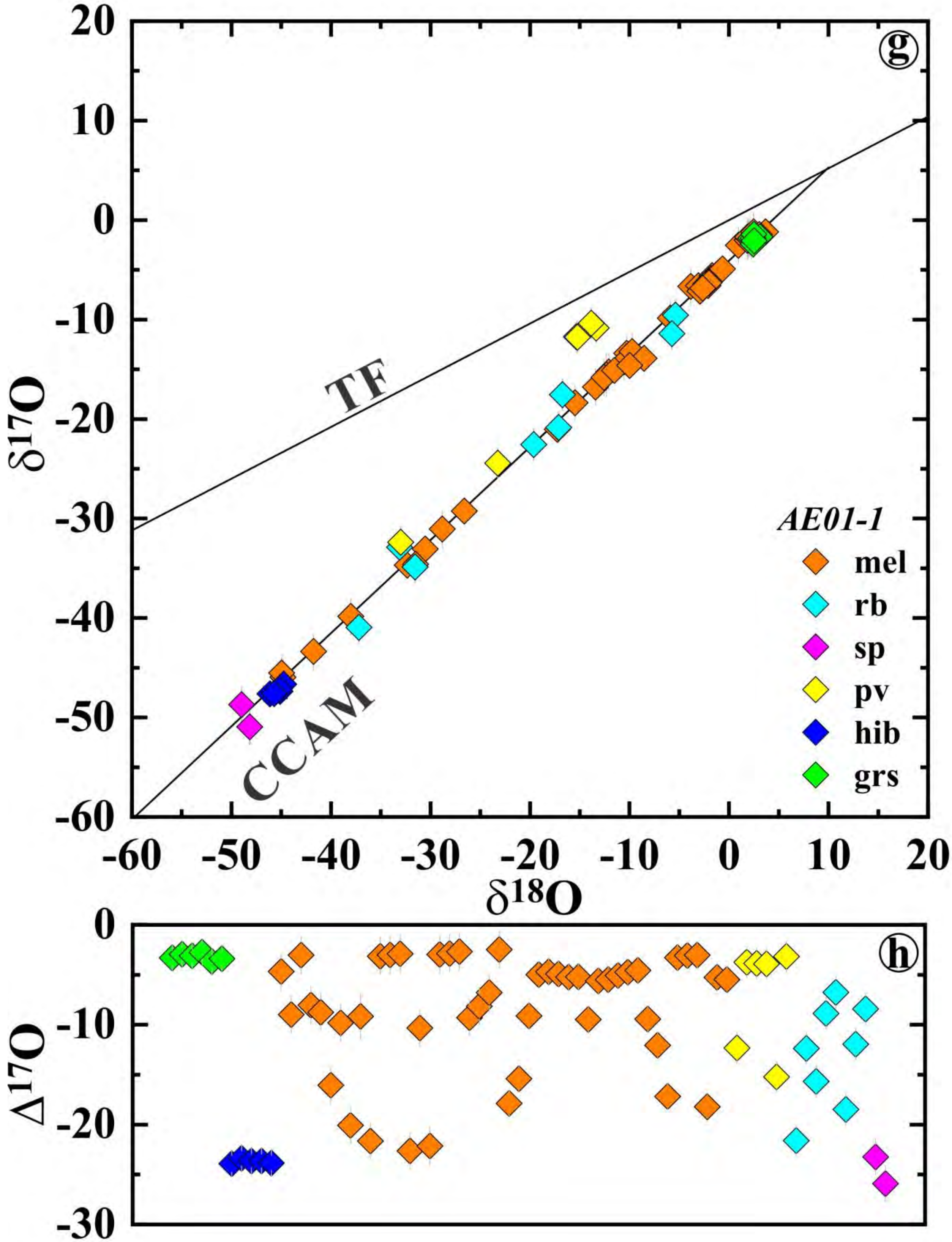
g
TF
CCAM
AE01-1
mel
rb
sp
pv
hib
grs
δ17O
δ18O
20
10
0
-10
-20
-30
-40
-50
-60
-60
-50
-40
-30
-20
-10
0
10
20
h
Δ17O
0
-10
-20
-30

529

**Figure 6.** (a, c, e, g) $\delta^{17}O$ *vs.* $\delta^{18}O$ and (b, d, f, h) $\Delta^{17}O$ of individual minerals in the rubinite-bearing CAIs from Efremovka and Allende. All rubinite-bearing CAIs have internally heterogeneous oxygen-isotope compositions. The terrestrial fractionation (TF) line and Carbonaceous Chondrite Anhydrous Mineral (CCAM) line are shown for reference.